

Th–U–total Pb monazite geochronology records Ordovician (444 Ma) metamorphism/partial melting and Silurian (419 Ma) thrusting in the Kåfjord Nappe, Norwegian Arctic Caledonides

GRZEGORZ ZIEMNIAK^{1,✉}, KAROLINA KOŚMIŃSKA¹, IGOR PETRÍK², MARIAN JANÁK²,
KATARZYNA WALCZAK¹, MACIEJ MANECKI¹ and JAROSŁAW MAJKA^{1,3}

¹Faculty of Geology, Geophysics and Environmental Protection, AGH — University of Science and Technology, Mickiewicza 30, 30-059 Kraków, Poland; [✉]ziemniak.grzegorz@gmail.com

²Earth Science Institute, Slovak Academy of Sciences, Dúbravská cesta 9, P.O. Box 106, 840 45 Bratislava 45, Slovakia

³Department of Earth Sciences, Uppsala University, Villavägen 16, 752-36 Uppsala, Sweden

(Manuscript received March 11, 2019; accepted in revised form November 14, 2019)

Abstract: The northern extent of the Scandinavian Caledonides includes the Skibotn Nappe Complex of still debated structural position. This paper is focused on part of this complex and presents new U–Th–total Pb monazite dating results for the migmatitic gneiss of the Kåfjord Nappe. The rocks show mineral assemblage of garnet+plagioclase+biotite+white mica+kyanite+rutile±K-feldspar±sillimanite. Thermodynamic modelling suggests that garnet was stable at P–T conditions of ca. 680–720 °C and 8–10 kbars in the stability field of kyanite and the rocks underwent partial melting during exhumation following a clockwise P–T path. This episode is dated to 444±12 Ma using chemical Th–U–total Pb dating of the Y-depleted monazite core. Second episode highlighted by growth of secondary white mica resulted from subsequent overprint in amphibolite and greenschist facies. Fluid assisted growth of the Y-enriched monazite rim at 419±8 Ma marks the timing of the nappe emplacement. Age of migmatization and thrusting in the Kåfjord Nappe is similar to the Kalak Nappe Complex, and other units of the Middle Allochthon to the south. Nevertheless, the obtained results do not allow for unambiguous definition of the tectonostratigraphic position of the Skibotn Nappe Complex.

Keywords: Scandinavian Caledonides, Skibotn Nappe Complex, migmatite, geochronology.

Introduction

The Caledonides in Scandinavia were formed as a result of closure of the Iapetus Ocean during the Ordovician, and the subsequent Silurian–Devonian collision between Laurentia and Baltica. The collision involved deep subduction of the Baltic margin beneath Laurentia (e.g., Gee 1975) and was followed by hinterland uplift, collapse of the orogen and emplacement of the allochthons onto the Baltoscandian platform (e.g., Gee et al. 2008).

Eastward translational movement of the succeeding nappes during the Caledonian Orogeny, up to several hundreds of kilometres, resulted in a distinctive tectonostratigraphy and formation of the Lower, Middle, Upper and the Uppermost allochthons (Roberts & Gee 1985). These allochthons were thrust onto the autochthonous sediments covering the crystalline Precambrian basement of the Baltic Shield, i.e., the Autochthon. The Lower and Middle allochthons comprise mostly parautochthonous basement and the Baltic margin sediments. The Upper Allochthon consists of Iapetus Ocean sediments, island arc and ophiolitic sequences. The Uppermost Allochthon is composed of rock units of Laurentian origin (e.g., Stephens & Gee 1989; Pedersen et al. 1992; Gee et al. 2008).

The main objective of this study was to investigate the metamorphism of the kyanite–garnet gneisses of the Kåfjord Nappe, a poorly characterized tectonic unit located in the Norwegian Arctic Caledonides (Figs. 1 and 2). We are presenting new geochronological constraints obtained using Th–U–total Pb dating of monazite. This work contributes to the existing geochronological database for the northernmost extent of the Scandinavian Caledonides.

Geological background

The Kåfjord Nappe is traditionally ascribed to the Upper Allochthon of the Norwegian Arctic Caledonides. This thrust sheet together with the overlying Nordmannvik Nappe and the underlying Vaddas Nappe, belong to the Skibotn Nappe Complex (Binns 1978) or Reisa Nappe Complex (Zwaan 1978; Fig. 2). In this region, the Middle Allochthon is represented by the Kalak Nappe Complex, of which the upper units are considered to be an equivalent to the Seve Nappe Complex farther south (Gayer et al. 1985; Ramsay & Sturt 1986; Andréasson et al. 1998; Siedlecka et al. 2004; Kirkland et al. 2007). The Kalak Nappe Complex underwent migmatization event dated to 702±5 Ma by the U–Pb zircon method, whereas

monazite reveal a scatter of U–Pb dates between 800 Ma to 600 Ma (Gasser et al. 2015). Chemical dating of monazite from granitic veins within the Helmsøy Shear Zone in the Kalak Nappe Complex yielded ages of 448 ± 7 Ma and 421 ± 7 Ma. U–Pb dating of zircon from the same locality gave a spread of dates from 470 Ma to 430 Ma (Kirkland et al.

2009). The Kalak Nappe Complex was intruded by the Halti Igneous Complex comprising ophiolitic rock assemblages at 434 ± 5 Ma (Vaasjoki & Sipila 2001) or between 445 and 435 Ma (Andréasson et al. 2003).

The Skibotn Nappe Complex consists of nappes of uncertain origin (Andresen 1988; Lindstrøm & Andresen 1992) that

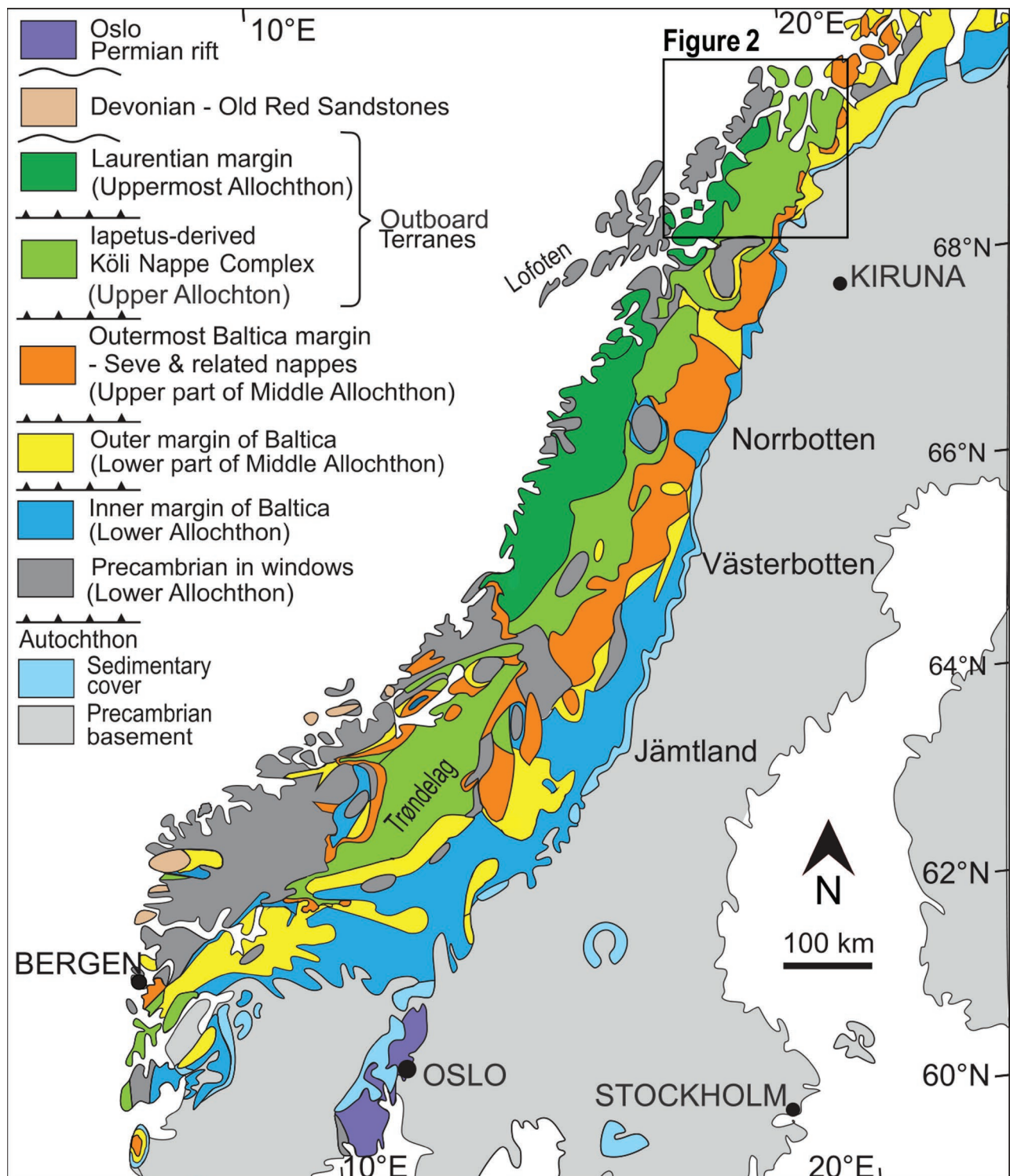


Fig. 1. Tectonostratigraphic map of the Scandinavian Caledonides modified after Gee et al. (2013).

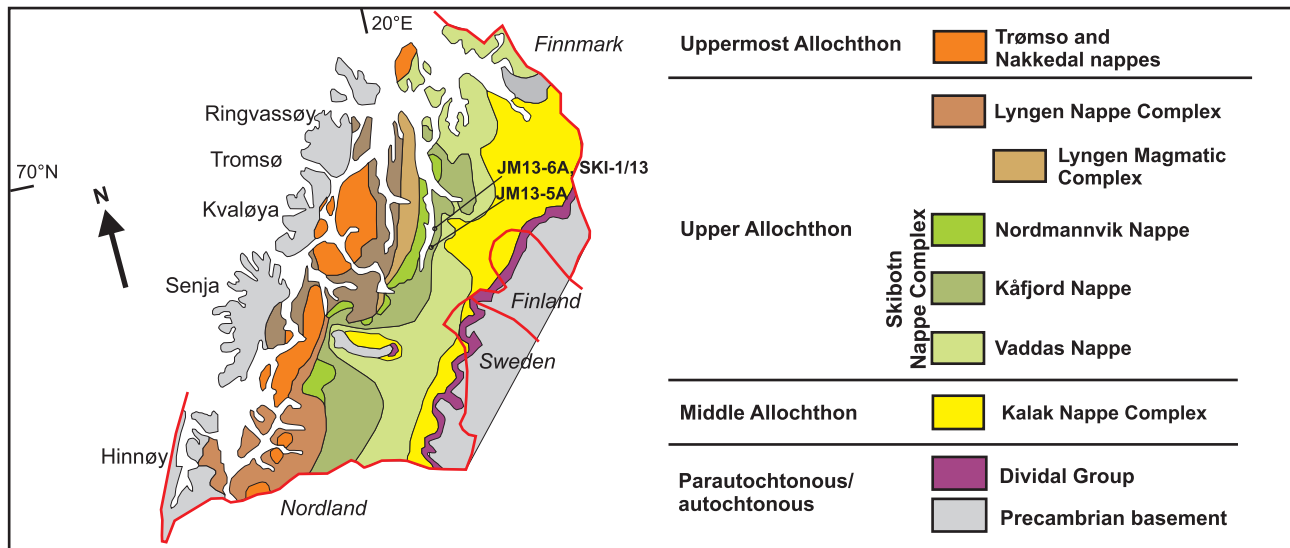


Fig. 2. Tectonostratigraphic map of the Tromsø area, modified after Janák et al. (2012) and marked sampling points. GPS coordinates of the samples JM13-5A ($69^{\circ}22'29.50''\text{N}$, $20^{\circ}13'42.05''\text{E}$); JM13-6A and SKI-1/13 ($69^{\circ}26'33.64''\text{N}$, $20^{\circ}17'59.55''\text{E}$).

may be affiliated to the Baltic margin (Lindahl et al. 2005). The coherent tectonometamorphic evolution of these nappes has been proposed based on lithological similarities and upward increase of metamorphic grade (Bergh & Andresen 1985; Andresen & Steltenpohl 1994).

The lowermost unit of the Skibotn Nappe Complex is the Vaddas Nappe composed of two subunits differing in origin, namely the Kvænangen Group and the overlying Oksfjord Group. The Kvænangen Group is interpreted as continental shallow water sequence consisting of marbles, quartzites and schists with amphibolite lenses and granites. This group varies in thickness, composition and metamorphic grade along the strike (Lindahl et al. 2005). Granitic gneisses of the Kvænangen Group were dated to 602 ± 5 Ma (Corfu et al. 2007). The Oksfjord Group lies unconformably on the Kvænangen Group (Ramsay et al. 1985) and is interpreted as a short-lived, transtensional basin associated with late Ordovician–early Silurian magmatism (Sturt & Roberts 1991; Lindahl et al. 2005). It consists of metasediments intercalated with amphibolites considered to be basaltic pillow lavas and gabbros. The Vaddas Nappe rocks were metamorphosed mostly under low amphibolite facies conditions, reaching kyanite stability field. In Arnøya, the pressure–temperature (P–T) conditions of metamorphism related to shearing were estimated to 11.7–13.0 kbar at 630 – 640 °C (Faber et al. 2019).

The Kåfjord Nappe has not been well studied so far. It is separated from the underlying Vaddas Nappe by the Cappis Thrust (Andresen 1988). The Kåfjord Nappe is characterized by high strain, extensive mylonitization and internal thrust faults dividing it into several sub-units. It is dominated by marbles, metapsammites and garnet-mica schists reaching high amphibolite facies metamorphic grade (Dallmeyer & Andresen 1992). In the upper level of the Kåfjord Nappe, mylonitic gneisses with boudinaged amphibolite layers and

granite bodies are exposed (Andresen 1988). $^{87}\text{Rb}/^{86}\text{Sr}$ dating of the Trollvik granite yielded an age of 452 ± 13 Ma (Dangla et al. 1978). Geochronological data for metapelites are limited to whole rock $^{87}\text{Rb}/^{86}\text{Sr}$ ages of 439 ± 5 Ma for non-migmatitic gneisses and 414 ± 3 Ma for migmatitic gneisses (Dangla et al. 1978). In Arnøya the P–T conditions for the peak of prograde metamorphism were constrained to 5.8–7.1 kbar at 590 – 610 °C, while subsequent amphibolite facies shearing reached 9.2–10.1 kbar at 580 – 605 °C (Faber et al. 2019).

The Kåfjord Nappe is overlain by the uppermost unit of the Skibotn Nappe Complex, namely the Nordmannvik Nappe. This nappe consists of polymetamorphic rocks which include mylonitic micaceous gneisses with garnet amphibolites, marbles, calc-silicates and ultramafic lenses (Andresen 1988). These rocks have undergone metamorphism in upper amphibolite facies, but relict granulite facies mineral assemblages are present as well (Bergh & Andresen 1985; Andresen 1988). P–T metamorphic conditions of ca. 9.2 kbar and 715 °C were estimated for the granulite assemblage at the Heia locality (Ellevold 1988). In Arnøya the peak metamorphic conditions were constrained to 9.4–11 kbar at 760 – 790 °C. The migmatization was dated to 441 ± 2 Ma and 439 ± 2 Ma using SIMS U–Pb dating on zircon from melanosome and leucosome, respectively (Faber et al. 2019). $^{87}\text{Rb}/^{86}\text{Sr}$ dating performed on metadiorites in the Heia locality yielded an age of 492 ± 5 Ma (Lindstrøm & Andresen 1992), while the emplacement of the Heia gabbro was dated to 435 ± 1 Ma using U–Pb ID-TIMS technique (Augland et al. 2014). Subsequent shearing was dated to 420 ± 4 Ma (Augland et al. 2014). Although the Nordmannvik Nappe is traditionally ascribed to the Upper Allochthon (Andresen 1988), some authors allow or even favour the possibility of its correlation with the Seve nappes of the Middle Allochthon, which would have to involve an out-of-sequence thrusting (Lindstrøm & Andresen 1992). Mafic and felsic intrusions emplaced at ca. 440–430 Ma within

the Skibotn Nappe Complex and the Kalak Nappe Complex led to the conclusion that both units at that time belonged to the same extensional basin developed along Baltoscandian margin (Andréasson et al. 2003). An alternative model for the extensional basin including the Skibotn Nappe Complex and part of the Kalak Nappe Complex, but developed along Laurentian margin was also proposed (Slagstad & Kirkland 2017).

The highest tectonic unit within the Upper Allochthon of the Troms area is the Lyngen Nappe Complex comprising the Koppangen Formation, the Lyngen Magmatic Complex and the Balsfjord Group. Tonalites of the Lyngen Magmatic Complex have been dated to 469 ± 5 Ma (Oliver & Krogh 1995) and 481 ± 6 Ma (Augland et al. 2014) using the U–Pb zircon system. $^{143}\text{Nd}/^{144}\text{Nd}$ isotope whole-rock analyses yielded composite back-arc-fore-arc affinity signatures of the Lyngen Magmatic Complex and suggest that it is either a lower crustal level of an incipient arc or an outer arc high (Kvassnes et al. 2004).

The Uppermost Allochthon comprises the Nakkedal Nappe Complex overlain by the Tromsø Nappe Complex of possible Laurentian origin (e.g., Stephens & Gee 1985). The Nakkedal Nappe Complex consists of metapelites and orthogneisses followed upwards by an amphibolitic and mafic–ultramafic magmatic complex and the Skattøra Migmatite Complex dated to 456 ± 4 Ma (U–Pb on titanite; Selbekk et al. 2000) and 449.5 ± 0.9 (U–Pb on zircon; ID-TIMS; Augland et al. 2014). The Tromsø Nappe Complex comprises various metasedimentary, metaigneous and metamorphic rocks including ultra-high-pressure eclogites and diamond-bearing gneisses (Ravna & Roux 2006; Janák et al. 2012, 2013). The eclogites were dated using the U–Pb method on zircon to 452.1 ± 1.7 Ma and their exhumation was inferred to have taken place between ca. 452 and 449 Ma (Corfu et al. 2003; Ravna & Rough 2006). An age of primary magmatic zircon from gneisses interlayering the eclogites was estimated to ca. 493 Ma (Corfu et al. 2003).

Analytical methods

Whole rock chemistry

The bulk composition of the samples was obtained by XRF following fusion of sample powders and $\text{LiBO}_2/\text{Li}_2\text{B}_4\text{O}_7$ at the Bureau Veritas Mineral Laboratories in Canada. The analytical results are presented in Table 1.

Mineral chemistry and element maps

For microprobe analysis of sample JM13-5A a JEOL Super Probe JXA-8230 Electron Probe Microanalyzer at Critical Elements Laboratory of the Department of Geology, Geophysics and Environmental Protection, AGH—University of Science and Technology in Kraków was used. A CAMECA SX-100 electron probe microanalyzer at the State Geological Institute of Dionýz Štúr in Bratislava was used for microprobe

analysis of sample JM13-6A. Operating conditions were as follows: 15 kV accelerating voltage, 20 nA beam current, counting time 20 s on peaks and beam diameter of 5 μm . The following standards were used for calibration of all detected silicates: orthoclase ($\text{Si K}\alpha$, $\text{K K}\alpha$), TiO_2 ($\text{Ti K}\alpha$), metallic Cr ($\text{Cr K}\alpha$), Al_2O_3 ($\text{Al K}\alpha$), fayalite ($\text{Fe K}\alpha$), rhodonite ($\text{Mn K}\alpha$), forsterite ($\text{Mg K}\alpha$), wollastonite ($\text{Ca K}\alpha$), albite ($\text{Na K}\alpha$). PAP corrections were applied for the matrix effects.

X-ray maps of garnet and monazite were acquired using the JEOL Super Probe at AGH in Kraków. The measurement conditions for garnet chemical maps were 15 kV and 100 nA. A fixed-step stage scan was used with step width of 5 μm and step counting times of 100 ms. Chemical maps were collected for $\text{Mg K}\alpha$, $\text{Ca K}\alpha$, $\text{Y L}\alpha$, and $\text{Mn L}\alpha$. The monazite chemical maps were acquired at 25 kV and 200 nA with fixed-step stage scan resolution of 0.2 μm and counting times of 100 ms per step for $\text{Y L}\alpha$, $\text{Th M}\alpha$ and $\text{Ce L}\alpha$.

Element ratios were determined from the cation distribution scans using XMapTools 2.4.3 (Lanari et al. 2014, 2019). Cut-off limits were selected to correspond with the spread of the values.

Mineral abbreviations in this article are according to Whitney & Evans (2010); WM — white mica. Analytical results are presented in Tables 2–4.

Th–U–total Pb monazite dating

The CAMECA SX-100 electron probe microanalyzer at the State Geological Institute of Dionýz Štúr in Bratislava was used for chemical dating of monazite. For the analysis of monazite counting times were increased to 80 s for U and 300 s for Pb to meet the requirements for trace element analysis. The beam current was adjusted to 180 nA and spots were measured with 3 μm beam diameter. The following standards were used for calibration: barite ($\text{S K}\alpha$), apatite ($\text{P K}\alpha$), GaAs ($\text{As L}\alpha$), ThO_2 ($\text{Th M}\alpha$), UO_2 ($\text{U M}\beta$), Al_2O_3 ($\text{Al K}\alpha$), YPO_4 ($\text{Y L}\alpha$), LaPO_4 ($\text{La L}\alpha$), CePO_4 ($\text{Ce L}\alpha$), PrPO_4 ($\text{Pr L}\beta$), NdPO_4 ($\text{Nd L}\beta$), SmPO_4 ($\text{Sm L}\beta$), EuPO_4 ($\text{Eu L}\beta$), GdPO_4 ($\text{Gd L}\alpha$), TbPO_4 ($\text{Tb L}\alpha$), DyPO_4 ($\text{Dy L}\beta$), HoPO_4 ($\text{Ho L}\beta$), ErPO_4

Table 1: Bulk chemical composition of analyzed samples.

	JM13-5A	JM13-6A
SiO_2	75.16	71.19
TiO_2	0.88	1.02
Al_2O_3	11.50	12.93
Fe_2O_3	4.47	5.70
MnO	0.02	0.09
MgO	1.72	2.61
CaO	0.97	0.97
Na_2O	0.76	1.26
K_2O	2.74	2.55
P_2O_5	0.08	0.18
LOI	1.50	1.30
Sum	99.78	99.71
* $\text{CaO}/\text{Al}_2\text{O}_3$	15.80	18.70

$\text{CaO}/\text{Al}_2\text{O}_3$ * ratio corrected for apatite.

Table 2: Representative chemical analysis of garnet. Structural formulae recalculated on the basis of 12 oxygens.

Sample ID	JM13-5A	JM13-5A	JM13-5A	JM13-5A	JM13-5A	JM13-5A	JM13-6A	JM13-6A	JM13-6A
Analysis	Grt 22	Grt 23	Grt 22	Grt 23	Grt 21	Grt 21	Grt 11	Grt B1	Grt 11
Text. pos.	Grt core	Grt core	Grt rim	Grt rim	Grt core	Grt rim	Grt core	Grt II core	Grt II rim
SiO₂	38.13	38.10	38.04	38.45	38.78	39.10	38.05	38.19	38.12
TiO₂	0.08	0.05	0.04	0.00	0.00	0.01	0.00	0.01	0.00
Al₂O₃	21.21	21.30	21.50	21.60	21.50	21.58	21.26	21.04	21.21
Cr₂O₃	0.05	0.00	0.02	0.00	0.00	0.00	0.00	0.03	0.02
FeO	28.67	27.87	30.72	31.34	31.60	30.62	32.07	32.52	33.10
MnO	2.68	3.01	1.21	0.96	0.71	0.29	2.51	2.76	2.29
MgO	2.82	2.59	4.18	4.29	4.20	4.17	5.14	4.58	4.71
CaO	6.18	6.21	3.58	3.59	3.82	4.88	2.11	2.38	1.73
Na₂O	0.01	0.00	0.00	0.02	0.02	0.00	0.03	0.02	0.05
K₂O	0.00	0.00	0.00	0.00	0.00	0.00	0.00	0.00	0.00
Total	99.83	99.13	99.29	100.25	100.63	100.65	101.22	101.52	101.49
Si	3.029	3.041	3.024	3.028	3.042	3.053	2.992	3.004	3.003
Ti	0.005	0.003	0.002	0.000	0.000	0.001	0.000	0.001	0.000
Al	1.987	2.005	2.015	2.006	1.988	1.987	1.971	1.951	1.970
Cr	0.003	0.000	0.001	0.000	0.000	0.000	0.000	0.002	0.001
Fe	1.905	1.861	2.042	2.064	2.073	2.000	2.109	2.139	2.181
Mn	0.180	0.204	0.081	0.064	0.047	0.019	0.167	0.184	0.153
Mg	0.334	0.308	0.495	0.504	0.491	0.485	0.603	0.537	0.553
Ca	0.526	0.531	0.305	0.303	0.321	0.408	0.178	0.201	0.146
Na	0.002	0.000	0.000	0.003	0.003	0.000	0.005	0.003	0.008
K	0.000	0.000	0.000	0.000	0.000	0.000	0.000	0.000	0.000
Total	7.971	7.953	7.966	7.971	7.966	7.953	8.025	8.021	8.015
X_{Alm}	0.647	0.641	0.698	0.703	0.707	0.687	0.690	0.699	0.719
X_{Prp}	0.113	0.106	0.169	0.172	0.167	0.167	0.197	0.175	0.182
X_{Grs}	0.179	0.183	0.104	0.103	0.109	0.140	0.058	0.066	0.048
X_{Sps}	0.061	0.070	0.028	0.022	0.016	0.007	0.055	0.060	0.050

(Er L β), TmPO₄ (Tm L α), YbPO₄ (Yb L α), LuPO₄ (Lu L β), SrTiO₃ (Sr L α), fayalite (Fe K α), wollastonite (Ca K α , Si K α), PbCO₃ (Pb M α). Empirically determined correction factors were applied to the following line overlaps: NdL α overlapped by CeL β , CeL β_4 ; GdL α by CeL γ , LaL γ_2 , NdL β_2 ; LuL β by DyL γ , DyL γ_2 , HoL γ , YbL β_2 ; EuL β by DyL α ; ErL β by EuL γ_3 , EuL γ_2 , GdL γ , LuL ν ; SmL α by CeL β_2 ; TmL α by SmL γ ; AsL α by NdM2N4, SmM γ , SmM3N4, TbM β and DyM α (Konečný et al. 2018). Spot analyses of monazite were corrected for mutual interferences and then the weighted average of apparent ages were calculated following the statistical method of Montel et al. (1996). Matrix effects were corrected using the PAP procedure.

Results

Petrography and textures

Three samples of migmatitic gneiss from the two localities within the Kåfjord unit were studied: JM13-5A (69°22'29.50" N, 20°13'42.05" E); JM13-6A and SKI-1/13 (69°26'33.64" N, 20°17'59.55" E). They are medium to fine grained, multiple leucocratic veins and pods, often with pale blue kyanite (Fig. 3), surrounded by distinctly darker layers dominated by macroscopically apparent streaks of reddish garnet and brown to black biotite. The gneisses are interbedded with

amphibolites and cut by later veins composed mainly of chlorite and epidote.

The M1 assemblage in the studied samples consists of garnet+plagioclase+biotite+quartz+kyanite±sillimanite±rutile±K-feldspar (Fig. 4a,b,c). This assemblage is locally found in the parts of the rock, which still show migmatitic structure, and as microlithons surrounded by the later S2 foliation. Leucocratic domains consist of quartz+plagioclase+garnet±kyanite±sillimanite and minor K-feldspar and ilmenite. The melanosome is dominated by the assemblage garnet+biotite+plagioclase+quartz+ilmenite±rutile.

The M2 assemblage in sample JM13-5A comprises quartz+white mica+biotite+plagioclase+rutile±clinzoisite and is variably altering migmatitic texture (Fig. 4d,e,f). The accompanying S2 foliation is defined by biotite, muscovite and quartz (Fig. 4d,f).

The M2 overprint in sample JM13-6A is manifested differently, being mainly characterized by growth of secondary transversal biotite and white mica replacing aluminosilicates. Chlorite, titanite and K-feldspar are growing in expense of biotite and garnet (Fig. 4g,h), while titanite is also replacing ilmenite and rutile. In sample SKI-1/13 rock-forming minerals are mostly fresh without alteration, however the rock is moderately sheared with mica deformation (mica fish).

Garnet porphyroblasts in all samples are subhedral to anhedral and vary from 0.4 to 3 mm in diameter. (Fig. 4c,d).

Table 3: Representative chemical analysis of biotite. Structural formulae recalculated on the basis of 11 oxygens.

Sample ID	JM13-5A b1	JM13-5A b4	JM13-5A m5	JM13-5A b3	JM13-5A b2	JM13-5A b10	JM13-6A M5	JM13-6A M13
Analysis	mx	mx	mx	mx	mx	mx	mx	mx
Text. pos.								
SiO ₂	38.92	39.08	39.31	39.60	39.57	37.51	37.22	36.82
TiO ₂	1.77	1.97	2.38	1.75	1.73	2.01	1.93	1.65
Al ₂ O ₃	19.66	18.41	18.12	18.53	18.76	18.88	17.94	18.67
Cr ₂ O ₃	0.03	0.03	0.03	0.01	0.01	0.04	0.05	0.03
FeO	14.08	14.57	15.05	15.06	15.38	15.66	17.10	17.08
MnO	0.00	0.00	0.00	0.00	0.01	0.01	0.02	0.05
MgO	12.16	11.65	11.80	12.22	12.14	12.30	11.93	12.50
CaO	0.09	0.01	0.00	0.00	0.00	0.03	0.01	0.03
Na ₂ O	0.38	0.34	0.30	0.26	0.28	0.32	0.27	0.28
K ₂ O	8.83	8.73	8.85	8.73	8.86	8.88	9.09	9.13
Total	94.58	94.77	95.83	96.16	96.74	95.62	95.62	96.26
Si	2.874	2.882	2.875	2.880	2.867	2.770	2.779	2.732
Ti	0.098	0.109	0.131	0.096	0.094	0.111	0.109	0.092
Al(VI)	1.116	1.118	1.125	1.120	1.133	1.230	1.221	1.268
Al(IV)	0.471	0.482	0.438	0.468	0.469	0.415	0.359	0.365
Cr	0.002	0.002	0.001	0.001	0.000	0.002	0.003	0.002
Fe	0.870	0.898	0.921	0.916	0.932	0.967	1.068	1.060
Mn	0.000	0.000	0.000	0.000	0.001	0.000	0.001	0.003
Mg	1.338	1.281	1.286	1.325	1.311	1.355	1.329	1.382
Ca	0.007	0.000	0.000	0.000	0.000	0.002	0.001	0.002
Na	0.054	0.048	0.042	0.037	0.040	0.045	0.039	0.040
K	0.832	0.821	0.826	0.810	0.819	0.837	0.866	0.864
Total	7.671	7.642	7.645	7.653	7.667	7.735	7.773	7.811
X _{Fe}	0.394	0.412	0.417	0.409	0.416	0.417	0.446	0.434

Table 4: Representative chemical analysis of white mica and plagioclase. Structural formulae recalculated on the basis of 11 and 8 oxygens, respectively.

Sample ID	JM13-5A f13	JM13-5A m6	JM13-5A p10	JM13-5A m7	JM13-5A m2	JM13-6A M3	JM13-6A M16	JM13-5A m3	JM13-5A f11	JM13-6A M4	JM13-6A M19
Analysis	mx	mx	mx	mx	mx	mx	mx	mx	mx	mx	mx
Text. pos.	Incl Ky										
SiO ₂	45.79	49.20	46.75	49.39	50.04	46.66	47.19	58.00	57.61	62.90	64.37
TiO ₂	0.96	1.04	1.05	0.90	0.96	0.77	0.67	0.01	0.00	0.00	0.00
Al ₂ O ₃	33.73	34.20	34.29	34.33	34.49	33.78	35.06	26.70	26.78	23.17	23.14
Cr ₂ O ₃	0.03	0.04	0.03	0.02	0.03	0.05	0.04	0.00	0.01	0.00	0.00
FeO	1.32	1.24	1.20	1.30	1.01	2.95	2.67	0.04	0.02	0.16	0.05
MnO	0.02	0.00	0.00	0.04	0.02	0.00	0.00	0.00	0.00	0.00	0.00
MgO	1.20	1.11	1.05	1.08	1.03	0.94	0.87	0.00	0.00	0.00	0.00
CaO	0.04	0.00	0.02	0.00	0.00	0.01	0.01	8.45	8.69	4.64	4.59
Na ₂ O	1.10	0.98	0.92	1.00	1.02	1.30	1.34	7.15	6.90	8.98	9.02
K ₂ O	9.67	9.72	9.85	9.65	9.35	8.74	8.95	0.07	0.09	0.06	0.08
Total	93.86	97.53	95.15	97.71	97.95	95.25	96.80	100.41	100.10	99.98	101.34
Si	3.092	3.177	3.107	3.182	3.202	3.110	3.090	2.577	2.572	2.788	2.818
Ti	0.049	0.051	0.052	0.044	0.046	0.039	0.033	0.000	0.000	0.000	0.000
Al	2.685	2.604	2.687	2.608	2.602	2.655	2.707	1.399	1.409	1.211	1.195
Cr	0.001	0.002	0.002	0.001	0.001	0.003	0.002	0.000	0.000	0.000	0.000
Fe	0.075	0.067	0.067	0.070	0.054	0.164	0.146	0.002	0.001	0.006	0.002
Mn	0.001	0.000	0.000	0.002	0.001	0.000	0.000	0.000	0.000	0.000	0.000
Mg	0.121	0.106	0.104	0.103	0.098	0.093	0.084	0.000	0.000	0.000	0.000
Ca	0.003	0.000	0.001	0.000	0.000	0.001	0.001	0.402	0.416	0.220	0.215
Na	0.144	0.123	0.118	0.124	0.127	0.169	0.170	0.616	0.597	0.772	0.765
K	0.833	0.801	0.835	0.793	0.764	0.744	0.748	0.004	0.005	0.000	0.000
Total	7.004	6.931	6.973	6.929	6.895	6.978	6.981	5.000	5.000	5.000	5.000
							X _{Ab}	0.605	0.589	0.778	0.781

The core contains numerous monomineral and polymimetallic inclusions composed mostly of quartz with minor plagioclase, chlorite, rutile and apatite. The inclusion trails highlight the S1 foliation and are aligned on planes within an angle towards to the S2 foliation planes (Fig. 4d). The rim contains fewer

inclusions, which are mostly monomineralic and represented by rutile, ilmenite and apatite. Garnet porphyroblasts are rotated and truncated by the S2 foliation.

Garnet in sample JM13-6A shows homogenous composition from core to rim: Alm₆₉₋₇₂Prp₁₇₋₂₀Grs₅₋₆Sps₄₋₆ and constant

X_{Fe} ($\text{Fe}/(\text{Fe}+\text{Mg})$) of 0.78–0.80 (Fig. 5a,b). In sample JM13-5A the composition of garnet core varies with size of the garnet. Relatively large garnet cores (>1.5 mm in diameter) have the composition $\text{Alm}_{64-68}\text{Prp}_{11-16}\text{Grs}_{13-18}\text{Sps}_{2-8}$ with X_{Fe} decreasing from 0.86 to 0.80 from core to rim (Fig. 5c,d). Compositional profiles and chemical maps in single grains of large garnet show increase of almandine and pyrope associated with decrease of spessartine and grossular from core to rim (Fig. 6a,b,c). The composition of the rim, starting at the characteristic Y annulus (Fig. 6d) is homogenous ($\text{Alm}_{69-70}\text{Prp}_{17-18}\text{Grs}_{10-12}\text{Sps}_{0-2}$) and has constant X_{Fe} of 0.80–0.81 (Fig. 5e,f). The composition of smaller garnet grains, with cores <1.5 mm in diameter, is homogeneous with no distinction between the core and the rim (Fig. 5c,d), and does not differ from the composition of the bigger garnet rims.

Biotite occurs as flakes parallel to both S1 and S2 foliation and as rare transversal blasts. X_{Fe} in biotite varies from 0.39 to 0.42 in the sample JM13-5A and from 0.43 to 0.45 in the sample JM13-6A. The lowest X_{Fe} values were recorded for biotite blasts in contact with garnet grains. The Ti content ranges from 0.09 to 0.13 a.p.f.u, while Al (IV) is 0.36–0.48 a.p.f.u in both samples.

White mica can be found in several textural positions: (i) as inclusions in garnet and kyanite, (ii) as sparse grains transversal to S1 foliation (Fig. 4c), (iii) as grains parallel to S2 foliation (Fig. 4d,e,f) and (iv) as grains transversal to S2 foliation (Fig. 4e). The textural position (iii) is the most common one. WM commonly replaces sillimanite, kyanite and/or biotite in various configurations. Silicon in white mica varies from 3.09 to 3.12 a.p.f.u for grains occupying most textural positions (i, ii, iii) and is slightly higher, from 3.18 to 3.20 a.p.f.u, for grains transversal to the S2 foliation (iv). For all samples, white mica shows a minor paragonite component with Na in the range from 0.12 to 0.17 a.p.f.u in all samples.

Kyanite forms subhedral to anhedral porphyroblasts with inclusion-rich cores and inclusion-poor rims. The inclusions are monomineralic and composed mainly of quartz with minor white mica (i), biotite and allanite. Kyanite is commonly truncated by the S2 foliation (Fig. 4f) and partly replaced by white mica (iii, iv) or sillimanite (Fig. 4h).

Sillimanite forms fibrolitic aggregates well dispersed in the matrix (Fig. 4a,b). Some of the aggregates locally replace garnet and kyanite.

Plagioclase occurs in the matrix and as intergrowths with quartz or K-feldspar. The composition of plagioclase differs between analyzed samples. X_{Ab} ($\text{Na}/(\text{Ca}+\text{Na}+\text{K})$) for plagioclase in the sample JM13-5A varies from 0.59 to 0.61, in the sample SKI-1/13 the $X_{\text{Ab}}=0.72$, while in the sample JM13-6A X_{Ab} is higher and ranges from 0.78 to 0.80. Plagioclase in intergrowths with K-feldspar is strongly albitic ($X_{\text{Ab}}=0.93-0.94$) with minor $X_{\text{Or}}=0.04-0.05$ ($X_{\text{Or}}=\text{K}/(\text{Ca}+\text{Na}+\text{K})$).

K-feldspar forms small (<0.5 mm) grains spread in leucosome and as intergrowths with albite. K-feldspar in leucosome shows $X_{\text{Ab}}=0.17$ and minor $X_{\text{An}}=0.02$.

Chlorite occurs in all samples in cracks parallel to the S2 foliation, mainly replacing biotite and garnet (Fig. 4g,h).



Fig. 3. Photograph of Kåfjord migmatitic gneiss with segregations of kyanite, sample SKI-1/13.

Titanite is present only in sample JM13-6A as tiny (<0.1 mm) aggregates of irregular shape associated with chlorite (Fig. 3G) and as coronas overgrowing ilmenite and rutile.

Other accessory minerals include clinzoisite, zircon, apatite, monazite, allanite, and tourmaline and pyrrhotite. A rare xenotime was also identified in sample SKI-1/13. Noteworthy, allanite and monazite occur together only in sample SKI-1/13.

Monazite is found in the matrix in samples JM13-6A and SKI-1/13 mostly enclosed in muscovite, quartz, biotite and plagioclase. In one case, in sample SKI-1/13, it was found within pyrrhotite, allanite and within garnet at the outer boundary of the inclusion-rich core. Monazite in sample JM13-6A is subhedral to euhedral and vary in size from 40 to 120 μm . In sample SKI-1/13 monazite is smaller, commonly rounded, isometric 5–15 μm in size. Larger grains (20–30 μm) may be elongated and irregular. Two samples of kyanite-garnet migmatitic gneiss (JM13-6A and SKI-1/13) from the same locality (Fig. 2) were chosen for monazite dating.

Chemical characteristics of monazite

BSE images of monazite grains in the sample JM13-6A reveal core to rim (Fig. 7a) or patchy zoning with irregular domains of various brightness (Fig. 7e). Monazite typically shows an irregular core to rim chemical variation that is expressed by the occurrence of two domains: (1) Y-depleted, Ce-enriched core, and (2) Y-enriched, Ce-depleted rim (Fig. 7b,c,f,g). Thorium displays irregular or (pseudo)oscillatory zoning (Fig. 7d,h), which does not correspond to the Y and Ce distribution. Thorium varies from 2.8 to 4.5 wt. % and U content is almost uniform (0.4–0.65 wt. %) in both core and rim. The patchy zoning does not comply with the Y, Th or Ce zoning (Fig. 7f–h).

The core and rim compositions are characterized by opposite trends on the Ca vs Y+HREE diagram (Fig. 8a) with rims enriched in Y+HREE. The Ca+P versus Si+Y+REE diagram (Fig. 8b) shows uniform trend for both groups, however the analyses performed within single monazite grains show

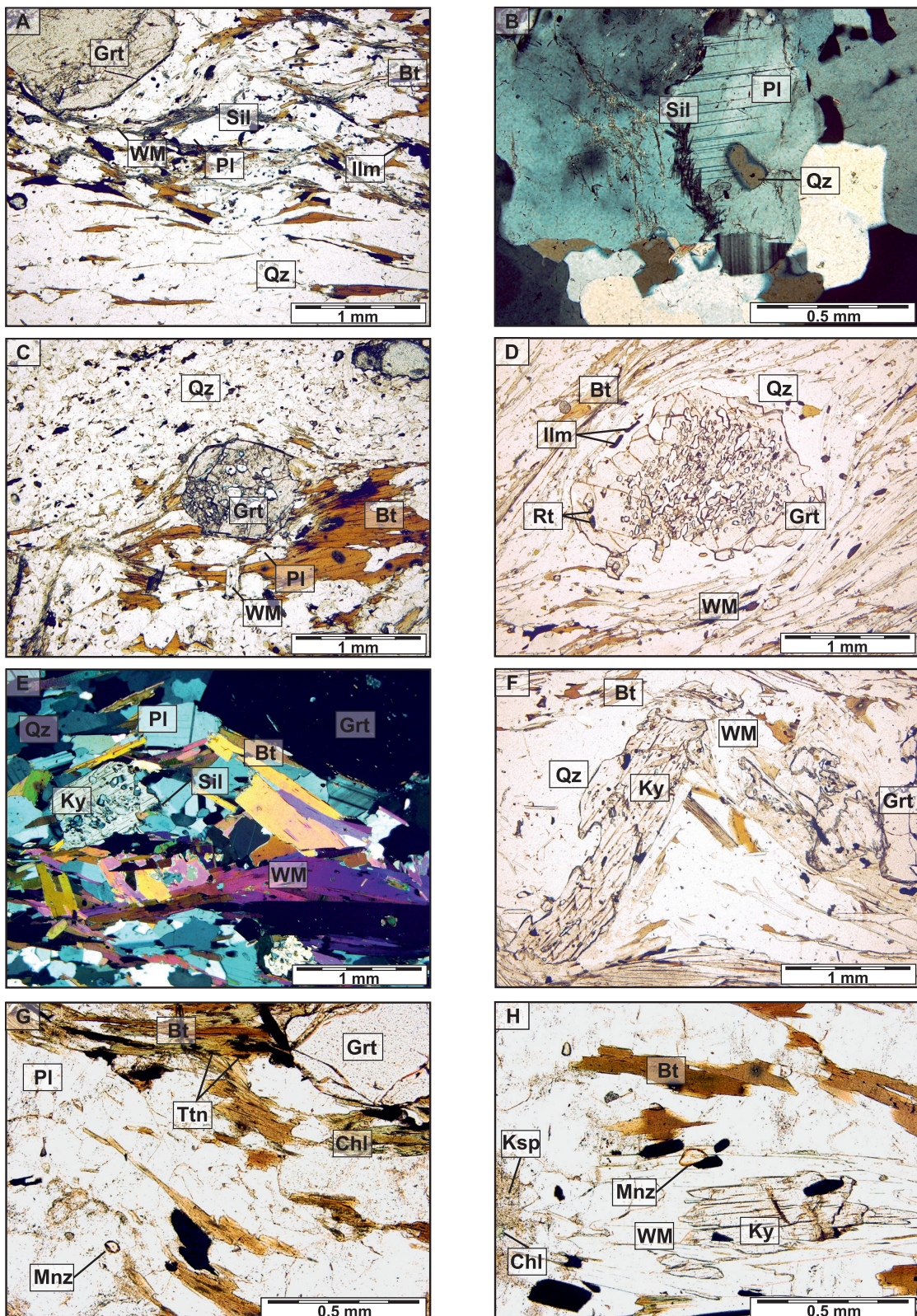


Fig. 4. Microphotographs of sample JM13-5A: **A** — assemblage M1 composed of quartz, garnet, plagioclase, biotite, sillimanite and ilmenite. White mica is replacing sillimanite; **B** — sillimanite fibrolite with plagioclase and quartz in leucosome; **C** — Garnet porphyroblast with plagioclase and biotite in melanocratic domain. White mica is growing transversal to S1 foliation; **D** — partially consumed garnet porphyroblast with multiple quartz inclusions in the core and only single inclusions of ilmenite and rutile in the rim; **E** — assemblage M2 composed of quartz, garnet, plagioclase, biotite, sillimanite and white mica. Kyanite is being replaced by sillimanite; **F** — pre-kinematic grain of kyanite truncated by S2 foliation defined by white mica and biotite; **G** — chlorite and biotite replacing garnet; biotite decomposing to chlorite, titanite and K-feldspar; **H** — chlorite and K-feldspar replacing biotite, white mica replacing kyanite.

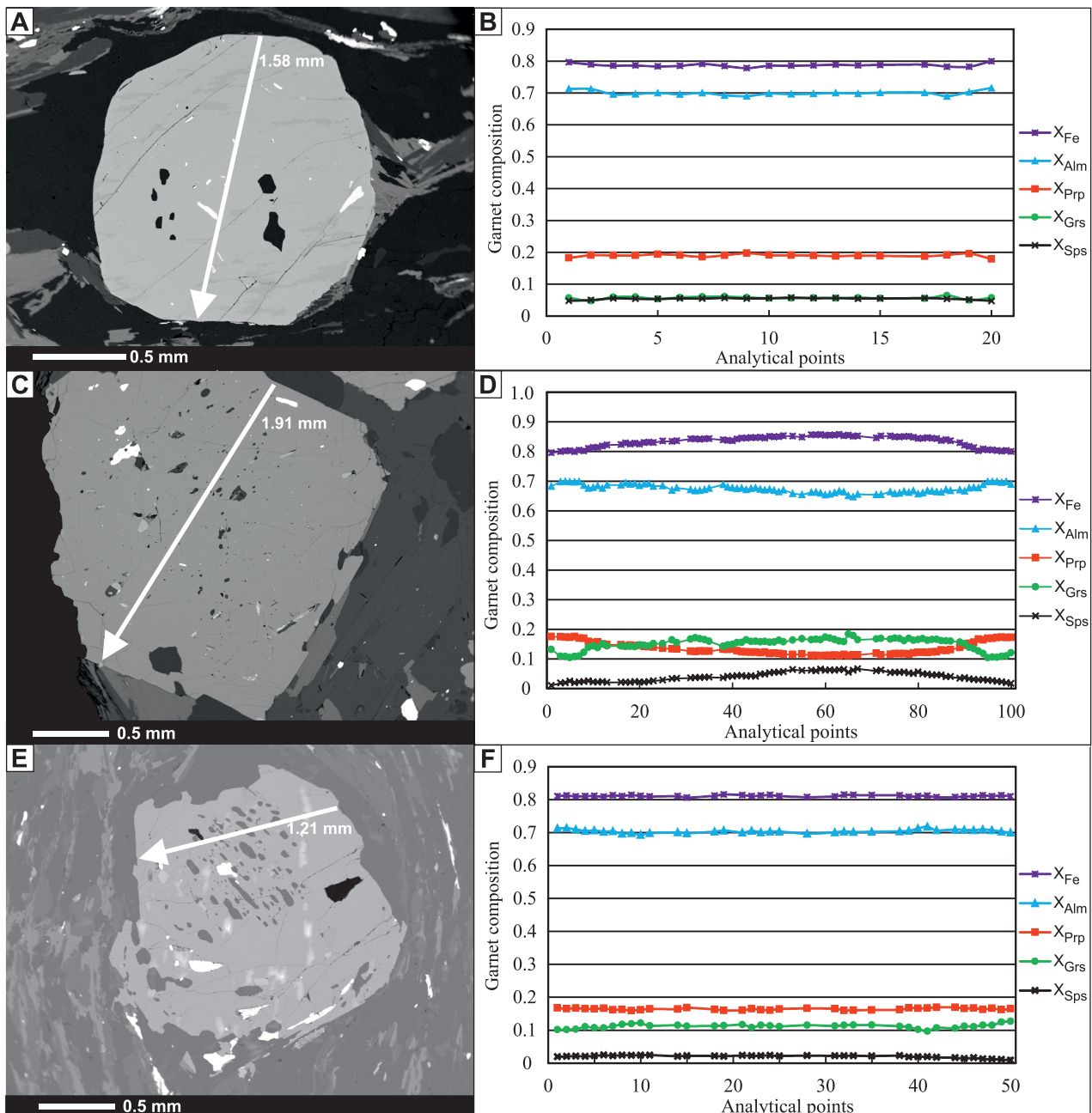


Fig. 5. Chemical composition of garnets in profiles. All garnets are characterized by inclusion rich cores and rims with only few inclusions. Sample JM13-6A: A — BSE image and B — compositional profile across garnet showing no chemical variations from core to rim. Sample JM13-5A: C — BSE image and D — compositional profile across garnet with larger core showing progressive zonation in the core, defined by decreasing X_{Sps} and X_{Fe} content towards the rim E — BSE image and F — Compositional profile across garnet with smaller core showing no chemical variations along the chemical profile. All garnets are characterized by inclusion rich cores and rims with only few inclusions.

enrichment in Ca+P from the core to the rim. Content of Monazite end member varies between 88–82 mol. %, cheralite between 7–12 mol. %, xenotime 2–6 mol. % and huttonite is about 1 mol. %. The REE patterns are steeper for the core than the rim with similarly pronounced negative Eu anomalies — Eu/Eu* from 0.76 down to 0.48 (Y is used as a proxy for Ho, heavier REEs are ignored due to their high scatter (Fig. 8c).

Monazite from the sample SKI-1/13 is characterised by complete analyses (Supplement) with low Th (2–5.5 wt. %

ThO₂), low U (0.2–1.5 wt. % UO₂). Monazite end member varies between 91–80 mol. %, cheralite between 5–12 mol. %, xenotime 5–7.5 mol. % and huttonite is about 1 mol. %. The REE patterns are steep with pronounced negative Eu anomalies (Eu/Eu* from 0.4 down to 0.12) and Y_N between 1000–2000 (Fig. 8c). The LREE from La to Sm are homogeneous. In general the variation of monazite composition is not distinctly related to textural features and position of analysed point within grain.

Results of dating

Sample JM13-6A: Electron microprobe single spot model dates ($n=21$) and chemical analysis for eight monazite grains are presented in the Table 5 and the Supplement. Calculation of all model dates yielded weighted average of 426 ± 6 Ma ($n=21$, MSWD=1.03, probability $p=0.42$; Fig. 9a). However, based on chemical maps of Ce and Y (Fig. 7b,c,f,g) two populations of monazite domains have been distinguished. A relationship between model dates of monazite domains and their Ce/Y relations are presented in Figure 9b. Monazite cores characterized by elevated Ce/Y ratio (14–27) with yttrium ranging from 0.9 to 1.75 wt. % yielded an average age of 444 ± 12 Ma ($n=6$, MSWD=0.89, $p=0.49$). Rims with lower Ce/Y (9–15) and higher Y content (1.6–2.5 wt. %) yielded an average age of 419 ± 8 Ma ($n=14$, MSWD=0.35, $p=0.98$). Based on chemical maps, one calculated date has been interpreted as mixed result and was omitted in the calculations of average ages.

Sample SKI-1/13: The sample is moderately rich in monazite: 18 crystals were dated by 41 points. Weighted average of all points give 430 ± 3.5 Ma with high MSWD=2.74 suggesting inhomogeneous monazite population. Therefore, deconvolution of the data was applied using Isoplot, which produced two ages 416 ± 6.9 (46 %, MSWD=1.3) and 442 ± 6.5

(54 %, MSWD=0.72). The age groups obtained from both samples are thus identical within errors. Monazite compositions divided according to deconvolution show that the younger population is relatively more homogeneous in terms of Y, Ce, U and Th compared to the older group (Fig. 9c,d).

Thermodynamic modelling

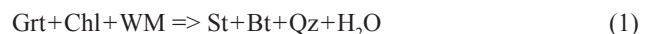
Phase diagram ($P-T$ pseudosection) was calculated for sample JM13-6A using the Perple_X software, version 6.8.6 (Connolly 1990, 2005) with the internally consistent thermodynamic dataset of Holland & Powell (2011; hp11ver.dat). The bulk rock composition (Table 1) was obtained from the whole rock analysis. Calculations were performed in the $\text{Na}_2\text{O}-\text{CaO}-\text{K}_2\text{O}-\text{FeO}-\text{MgO}-\text{Al}_2\text{O}_3-\text{SiO}_2-\text{H}_2\text{O}-\text{TiO}_2$ (NCKFMASHT) system assuming water-saturated conditions and partial melting. Solution models of garnet, white mica, biotite, cordierite (White et al. 2014), sanidine (Thompson & Hovis 1979), plagioclase (Newton et al. 1980), and melt (Holland & Powell 2001) were used as available from the Perple_X datafile (solution_model.dat).

The calculated phase diagram (Fig. 10) shows that compositional isopleths of garnet ($X_{\text{Mg}}^{\text{Grt}}$, $X_{\text{Ca}}^{\text{Grt}}$, $X_{\text{Fe}}^{\text{Grt}}$) and biotite ($X_{\text{Fe}}^{\text{Bt}}$) corresponding to the measured ones (Tables 1 and 2, Fig. 5B) intersect in the stability field of garnet+plagioclase+biotite+white mica+kyanite+rutile, constraining the $P-T$ conditions of garnet equilibration at 8–10 kbar and 680–720 °C. Garnet is unstable below ca. 8 kbars and 700 °C. Partial melting likely occurred at water saturated conditions during rock exhumation from the kyanite to the sillimanite stability field following a clockwise $P-T$ path (Fig. 10).

Discussion

Metamorphic evolution

In all samples inclusion-rich garnet core has irregular shape suggesting that the garnet core was partly resorbed before growth of the rim. Garnet resorption and regrowth in medium pressure metapelites is associated with staurolite-in and staurolite-out reactions that can be written as follows (Spear 1988):



Minor back-diffusion of Mn in the outermost part of the garnet core preceding Y-annulus in the rim (Fig. 6b,d) is characteristic for two stage garnet growth in staurolite to kyanite zone of amphibolite facies (Pyle & Spear 1999). In the medium-pressure metapelites, kyanite growth might be responsible for garnet consumption according to the reaction (Spear 1988):



Kyanite core contains multiple inclusions of quartz and white mica involved in the reaction (3). Kyanite rim was

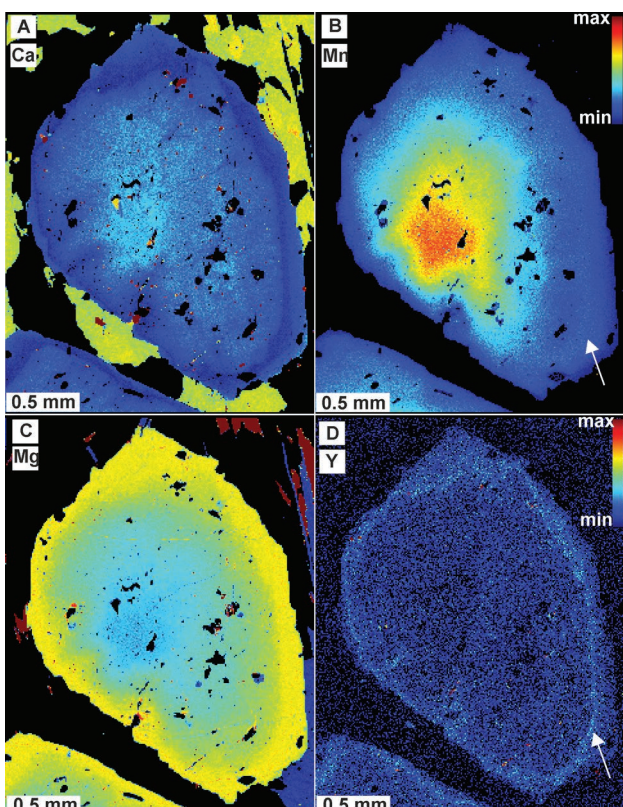


Fig. 6. Electron microprobe X-ray chemical maps of garnet in sample JM 13-5A. Concentration of elements **A** — Ca, **B** — Mn, **C** — Mg, **D** — Y, in not fully homogenized garnet showing progressive zoning pattern in the core. Boundary between core and rim is marked by a small Mn enrichment an Y-annulus (white arrows).

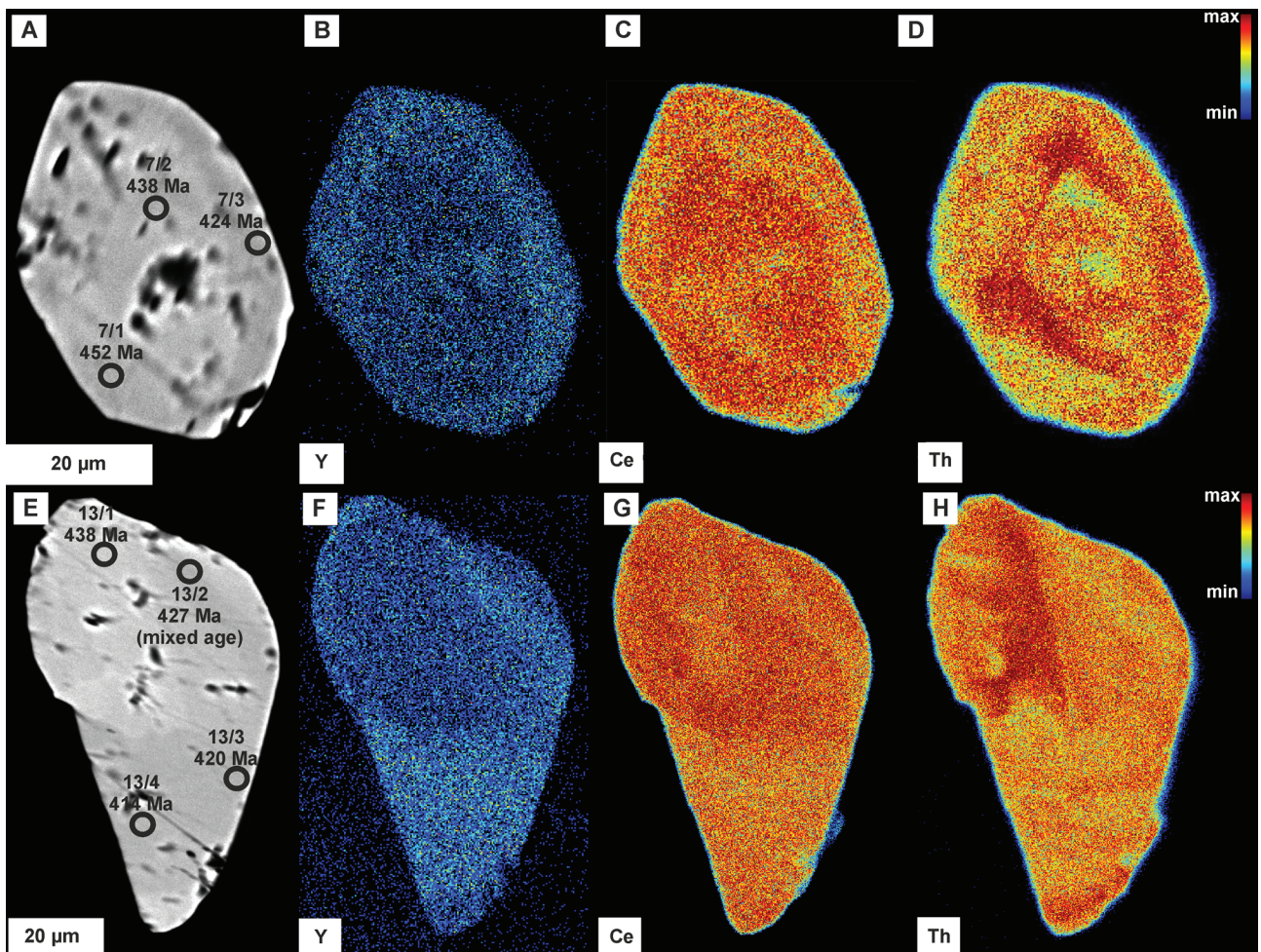
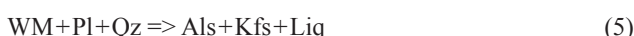


Fig. 7. BSE images and chemical maps of monazites: **A** — BSE image of monazite 7 characterized by core to rim zoning. Chemical map of **B** — Y, **C** — Ce, **D** — Th content in monazite 7. **E** — BSE image of monazite 13 characterized by patchy zoning with irregular domains of various brightness. Chemical map of **F** — Y, **G** — Ce, **H** — Th content in monazite 13. Warmer colours correspond to higher concentration of an element. Monazite core is Y-depleted, Ce-enriched in contrast to Y-enriched, Ce-depleted rim. Th displays irregular or (pseudo)oscillatory zoning.

produced on the prograde P-T path by muscovite dehydration reaction, which can be written as one of the following (Indares & Dunning 2001):



Reactions (4) and (5) are predicted by thermodynamic modelling within the estimated P-T space of 8–10 kbar and 680–720 °C for peak metamorphic conditions. The rare abundance of K-feldspar might be explained by reversed reaction (5) on the retrograde path. Formation of white mica on the early retrograde path and during M2 overprint might have led to nearly complete exhaustion of K-feldspar (M1).

Elevated temperature resulted in homogenization of the garnet composition (Spear 1988). Nevertheless, preservation of garnet zoning in migmatitic rocks mainly depends on the time of high-T diffusion, but also the size of the garnet (e.g., Tracy et al. 1976; Spear 1988; Caddick et al. 2010). For sample JM13-5A the high temperature event caused homogenization

of the smaller garnet cores characterized by flat chemical profiles (Fig. 5b), whereas larger garnet cores (>1.5 mm) were affected by diffusion (Figs. 4a, 5a–d), but retained some of the information about chemical trends during primary growth. These garnet cores are characterized by progressive garnet zoning with decreasing X_{Fe} and X_{Sp} .

Retrogressive reactions observed in both samples resulting in biotite+sillimanite overgrowths on garnet and white mica replacing kyanite, sillimanite and feldspars indicate reversal of the reaction (5). All generations of white mica occur only in textural positions that suggest growth along the retrograde path.

This early stage of nappe emplacement resulted in shear-related foliation and minor retrogression affecting already existing fabric. Garnet and kyanite porphyroblasts were rotated and truncated by S2 foliation (Fig. 4d,f). Chloritization of garnet and biotite as well as sericitization of plagioclase occurred at the final stage of decompression, probably aided by fluids.

Monazite geochronology

Nearly all monazites are located in the matrix, which makes it hard to assess at which point along the rock's evolutionary path they were formed. Additionally, the monazite REE

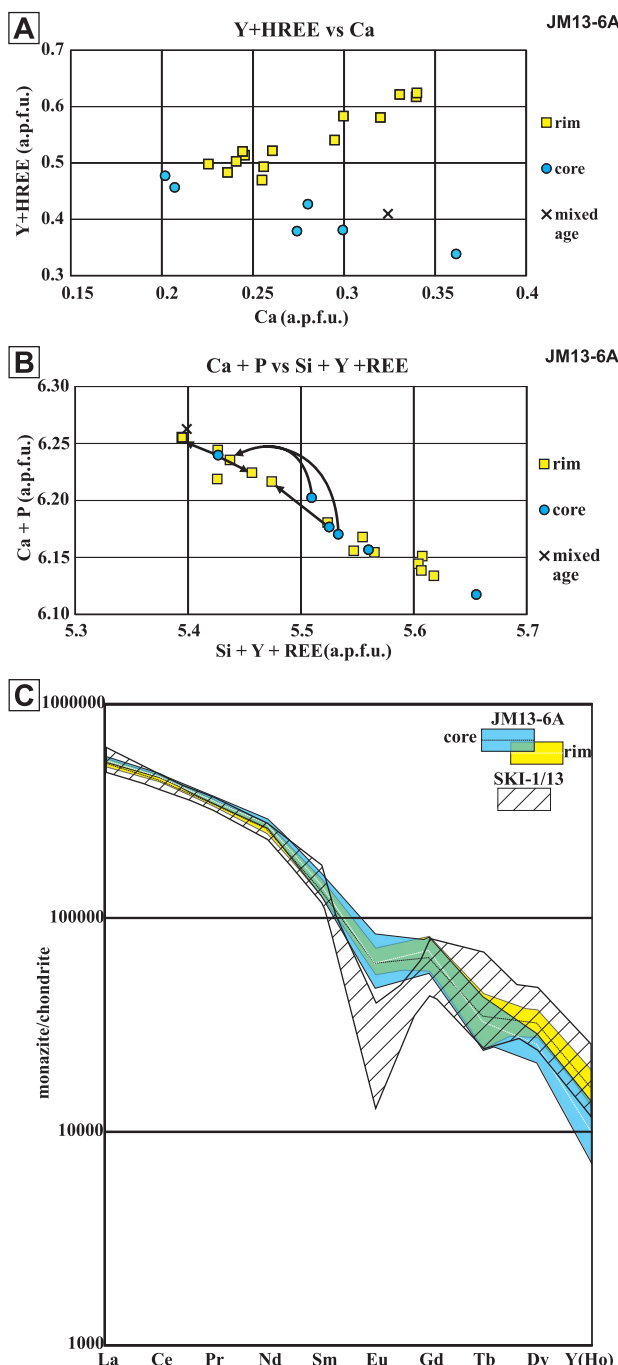


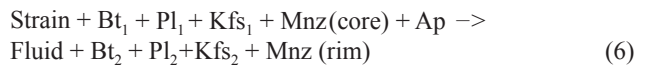
Fig. 8. — Monazite Y+HREE content versus Ca content presenting opposite trends for monazite core and rim in sample JM13-6A; **B** — Ca+P versus Si+Y+REE diagram, arrows highlight the chemical variation between the core and the rim within single grains in sample JM13-6A; **C** — Normalized REE patterns for monazite in samples JM13-6A and SKI-1/13. In sample JM13-6A steeper REE patterns in monazite core compared to less steep patterns in the rim. Dashed lines represent the average REE pattern for core and rim.

patterns differ between the samples JM13-6A and SKI-1/13 in terms Eu/Eu* anomaly and HREE content (Fig. 8c). This difference suggests, that the chemical composition of the monazite in the rock is strongly related to overall REE budget of the rock, or the chemical composition of monazite precursor (e.g., Janots et al. 2008). Monazite in sample SKI-1/13 is chemically less homogenous than in sample JM13-6A and does not show any correlation of chemical composition and obtained ages. In the sample JM13-6A monazite shows distinct zonation between cores and rims, which allows for potential interpretation of the obtained monazite ages. Main difference between the cores and rims is related to Y content that is governed by the stability of garnet, i.e., the main Y sink in metapelites of high amphibolite facies (e.g., Pan 1997; Pyle & Spear 1999). The cores characterized by higher Ce and lower Y were formed probably along the prograde part of the P-T path, in the presence of garnet. Therefore, the timing of prograde metamorphism/partial melting is constrained to 444 ± 12 Ma based on Y-poor monazite domains.

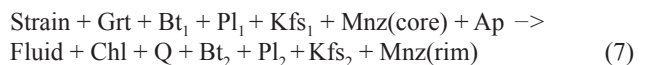
The monazite rims are characterized by lower Ce and higher Y and were probably formed under P-T conditions allowing for garnet decomposition and, in turn, a release of Y to the system. This is supported by thermodynamic modelling which predicts that garnet was unstable at P-T conditions below 8 kbars and 700 °C (Fig. 10).

The high-Y monazite rim formation ca. 419 Ma might be tied to low-pressure overprint and formation of S2 foliation during the Scandian event. Chemical characteristics of sample JM13-6A shows relatively high $\text{Al}_2\text{O}_3/\text{CaO}$ ratio of 18.7 (Table 1.), which can stabilize monazite in greenschist facies (see e.g., Spear 2010), thus a greenschist facies overprint would not necessarily result in monazite reacting to allanite.

Garnet decomposition to biotite and chlorite under greenschist facies conditions may cause release of Y, which subsequently is incorporated in monazite in xenotime-absent rocks. Greenschist facies monazite has been noted before (e.g., Franz et al. 1996; Pyle et al. 2001) including even idioblastic crystals associated with shear zones (Lanzirotti & Hanson 1996). Furthermore, shearing might be responsible for producing internal fluid through recrystallization of biotite according to the reaction such as proposed by Dumond et al. (2008):



Introducing garnet into the reaction (6) that produces fluid required for chlorite formation would result in the following reaction:



Monazite rim formed according to this garnet consuming reaction would be enriched in Y+HREE (Fig. 8a,c). Enrichment in Ca+P from core to rim as observed in single monazite grains (Fig. 8b) supportsapatite dissolution with Ca+P and

Table 5: Measured and corrected Th, U, Pb concentrations, Th* values and ages for dated monazites from samples JM13-6A (1–21) and SKI-1/13 (22–49 thin section 1, 50–62 thin section 2)

No	Analysis	Th (wt. %)	Th 2σ	U (wt. %)	U 2σ	Pb (wt. %)	Pb 2σ	Y (wt. %)	Ce (wt. %)	Th*	Th/U	Ce/Y	Age (Ma)	Error (Ma)
1	mnz1/1	3.7653	0.0358	0.5003	0.0131	0.1013	0.0057	2.41	22.86	5.40	6.92	9.49	419	28
2	mnz1/2	3.6824	0.0354	0.5855	0.0135	0.1030	0.0057	2.35	23.06	5.60	5.86	9.81	412	27
3	mnz4/2	3.0995	0.0319	0.4360	0.0128	0.0916	0.0057	1.50	23.76	4.53	6.57	15.81	452	33
4	mnz7/1	3.6126	0.0349	0.4429	0.0130	0.1025	0.0057	1.28	24.31	5.07	7.45	18.93	452	30
5	mnz7/2	3.9228	0.0367	0.4015	0.0128	0.1026	0.0057	1.09	24.09	5.24	8.78	22.16	438	29
6	mnz7/3	4.2391	0.0387	0.5868	0.0136	0.1169	0.0058	2.34	22.71	6.16	6.67	9.72	424	25
7	mnz13/1	4.4156	0.0396	0.5456	0.0133	0.1214	0.0058	0.91	23.57	6.20	7.40	26.04	438	25
8	mnz13/2	3.8236	0.0361	0.4357	0.0129	0.1002	0.0057	1.27	23.45	5.25	7.96	18.52	427	29
9	mnz13/3	3.9365	0.0369	0.5827	0.0135	0.1096	0.0058	2.37	22.72	5.84	6.26	9.60	420	26
10	mnz13/4	3.6535	0.0352	0.5289	0.0132	0.0997	0.0057	2.14	22.90	5.38	6.40	10.71	414	28
11	mnz14/1	3.3493	0.0334	0.4990	0.0131	0.0959	0.0057	1.92	23.31	4.98	6.23	12.12	431	30
12	mnz14/2	3.4442	0.0339	0.3776	0.0127	0.0887	0.0057	0.96	24.12	4.68	8.25	25.18	424	32
13	mnz15/1	2.8660	0.0305	0.4775	0.0130	0.0927	0.0057	1.73	24.54	4.43	5.61	14.22	468	34
14	mnz16/1	3.1886	0.0324	0.5730	0.0133	0.0912	0.0057	1.77	23.82	5.06	5.23	13.46	404	30
15	mnz16/2	3.9535	0.0369	0.5243	0.0132	0.1060	0.0057	1.62	23.67	5.67	6.93	14.59	419	27
16	mnz16/3	3.0521	0.0315	0.4410	0.0128	0.0839	0.0057	1.68	23.17	4.50	6.41	13.82	417	33
17	mnz16/4	3.3681	0.0335	0.5956	0.0135	0.1021	0.0057	1.81	23.50	5.32	5.31	13.01	430	29
18	mnz18/1	3.5382	0.0345	0.4134	0.0128	0.0952	0.0057	1.84	23.01	4.89	7.79	12.48	435	31
19	mnz18/2	3.4715	0.0341	0.3832	0.0126	0.0891	0.0057	1.75	23.24	4.73	8.20	13.31	422	32
20	mnz18/3	3.6388	0.0351	0.3792	0.0126	0.0906	0.0057	1.80	23.28	4.88	8.64	12.94	415	31
21	mnz18/4	3.5282	0.0345	0.5538	0.0133	0.0974	0.0057	1.86	22.99	5.34	5.93	12.33	408	28
22	mnz1/1	3.6892	0.0360	0.9735	0.0149	0.1346	0.0059	2.40	22.76	6.88	3.79	9.47	438	19
23	mnz1/2	3.1956	0.0330	1.0498	0.0151	0.1212	0.0058	1.93	23.26	6.63	3.04	12.05	410	19
24	mnz2/1	3.3362	0.0339	1.0451	0.0152	0.1286	0.0059	2.18	23.25	6.76	3.19	10.64	427	20
25	mnz3/1	2.4114	0.0281	0.3616	0.0127	0.0727	0.0057	1.95	24.50	3.60	6.67	12.58	452	35
26	mnz3/2	3.3659	0.0340	0.5499	0.0134	0.0924	0.0057	2.47	23.32	5.16	6.12	9.43	401	25
27	mnz4/1	2.9351	0.0315	0.4281	0.0128	0.0840	0.0053	1.57	21.35	4.34	6.86	13.62	433	27
28	mnz4/2	2.9985	0.0317	0.9568	0.0148	0.1207	0.0058	1.99	22.66	6.14	3.13	11.36	441	21
29	mnz4/3	1.2736	0.0211	0.2227	0.0122	0.0407	0.0055	1.93	24.74	2.00	5.72	12.81	454	61
30	mnz5/1	4.0937	0.0385	1.4564	0.0166	0.1663	0.0061	1.84	22.61	8.86	2.81	12.30	421	15
31	mnz6/1	3.5413	0.0351	0.7819	0.0143	0.1150	0.0059	2.54	22.79	6.10	4.53	8.98	422	21
32	mnz6/2	3.5188	0.0349	0.7838	0.0143	0.1164	0.0059	2.51	22.96	6.09	4.49	9.14	428	21
33	mnz6/3	3.7328	0.0363	0.6919	0.0140	0.1153	0.0059	2.23	23.10	6.00	5.40	10.36	430	22
34	mnz6/4	3.6830	0.0359	0.6704	0.0139	0.1120	0.0057	2.14	23.01	5.88	5.49	10.74	426	22
35	mnz7/1	3.2500	0.0333	0.8535	0.0145	0.1244	0.0059	2.08	23.44	6.05	3.81	11.30	460	22
36	mnz7/2	3.4745	0.0347	0.8571	0.0145	0.1174	0.0059	2.09	23.17	6.28	4.05	11.06	419	21
37	mnz8/1	3.0968	0.0324	0.6752	0.0139	0.1078	0.0059	2.08	23.84	5.31	4.59	11.47	454	25
38	mnz8/2	4.6593	0.0421	1.1358	0.0157	0.1677	0.0061	2.57	22.10	8.39	4.10	8.60	448	16
39	mnz8/3	4.5077	0.0411	1.1661	0.0157	0.1612	0.0061	2.41	22.12	8.33	3.87	9.20	433	16
40	mnz9/1	3.3129	0.0339	1.0904	0.0155	0.1301	0.0060	2.09	22.99	6.88	3.04	11.02	424	19
41	mnz9/2	2.3985	0.0283	0.5728	0.0135	0.0835	0.0057	3.34	22.36	4.28	4.19	6.70	437	30
42	mnz10/1	2.3052	0.0275	0.4534	0.0131	0.0769	0.0057	2.01	24.14	3.79	5.08	12.04	454	33
43	mnz11/1	2.0105	0.0257	0.8330	0.0144	0.0801	0.0058	2.37	23.96	4.73	2.41	10.09	380	27
44	mnz11/2	3.0303	0.0319	0.9767	0.0147	0.1218	0.0058	2.47	22.98	6.23	3.10	9.30	438	21
45	mnz12/1	4.1083	0.0385	0.9021	0.0146	0.1277	0.0059	2.62	22.68	7.06	4.55	8.66	405	19
46	mnz12/2	2.4195	0.0281	0.5465	0.0133	0.0849	0.0057	2.07	24.01	4.21	4.43	11.58	451	30
47	mnz12/3	3.4540	0.0344	0.6932	0.0138	0.1082	0.0057	2.25	23.27	5.72	4.98	10.32	423	22
48	mnz13/1	3.4458	0.0343	0.8367	0.0143	0.1151	0.0058	2.16	22.95	6.18	4.12	10.63	417	21
49	mnz13/2	3.3251	0.0338	1.0420	0.0152	0.1324	0.0060	2.90	22.33	6.74	3.19	7.70	440	20
50	mnz1/1	3.3423	0.0338	0.9188	0.0147	0.1222	0.0059	2.02	23.21	6.35	3.64	11.51	431	21
51	mnz1/2	3.4570	0.0346	0.9635	0.0149	0.1336	0.0059	2.03	22.89	6.62	3.59	11.30	452	20
52	mnz1/3	4.3886	0.0403	0.9400	0.0149	0.1385	0.0060	2.65	21.98	7.47	4.67	8.29	416	18
53	mnz1/4	3.0326	0.0322	0.6481	0.0139	0.0938	0.0059	2.05	23.41	5.15	4.68	11.42	408	25
54	mnz2/1	2.4376	0.0283	0.5302	0.0133	0.0775	0.0057	2.11	23.85	4.17	4.60	11.30	416	30
55	mnz2/2	3.5467	0.0353	0.6867	0.0141	0.1186	0.0059	1.96	22.73	5.80	5.16	11.58	457	23
56	mnz3/1	1.7362	0.0241	0.1910	0.0123	0.0443	0.0056	1.77	24.61	2.36	9.09	13.90	419	53
57	mnz3/2	2.3440	0.0277	0.4864	0.0132	0.0776	0.0057	1.87	23.78	3.94	4.82	12.73	441	32
58	mnz3/3	3.0169	0.0319	0.4827	0.0132	0.0882	0.0058	2.93	22.61	4.60	6.25	7.73	429	28
59	mnz4/1	3.5776	0.0352	0.6350	0.0137	0.0976	0.0057	2.54	23.14	5.65	5.63	9.11	387	23
60	mnz4/2	5.4159	0.0465	0.9448	0.0149	0.1713	0.0061	2.81	21.03	8.52	5.73	7.47	450	16
61	mnz5/1	2.5235	0.0288	0.4309	0.0129	0.0698	0.0057	2.09	23.50	3.93	5.86	11.27	398	32
62	mnz5/2	3.5615	0.0351	0.4859	0.0132	0.1050	0.0058	2.12	22.55	5.16	7.33	10.66	455	25

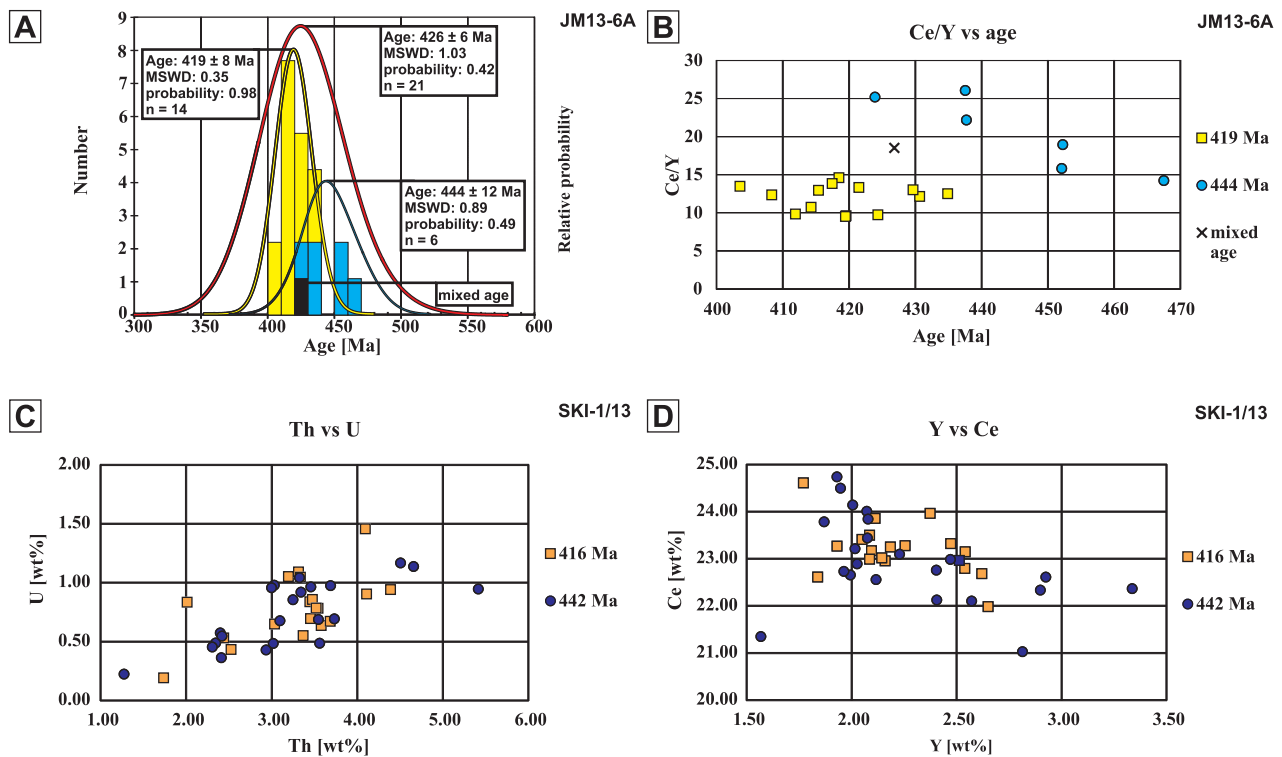


Fig. 9. A — Cumulative probability plot, with histogram, of monazite model dates; B — monazite model dates versus Ce/Y ratio. Monazite core (444 Ma) is characterized by higher Ce/Y than monazite rim (419 Ma). C — Th vs U correlation of the two age monazite populations. D — Ce vs Y correlation of the two age monazite populations.

Si+Y+REE exchange according to the strain induced reaction (7) (Harlov et al. 2005). Overall, monazite chemistry and textural observations support fluid assisted growth of the 419 ± 8 Ma monazite rim during greenschist facies overprint related to the nappe emplacement.

Tectonic implications

The obtained monazite ages of ca. 444 Ma and ca. 419 Ma are consistent within the errors with the previous whole rock $^{87}\text{Rb}/^{86}\text{Sr}$ ages of Dangla et al. (1978). Timing of migmatization event recorded by zircon in the Nordmannvik Nappe i.e., 441 ± 1 Ma and 439 ± 2 Ma (Faber et al. 2019) is similar to reported herein. Also, the age constrains on shearing from the Heia locality of 420 ± 4 Ma (Augland et al. 2014) support the uniform metamorphic evolution of the Skibotn Nappe Complex. Comparable to the data presented here are the results of monazite dating from the Helmsøy shear zone in the Kalak Nappe Complex, where the ages of 448 ± 7 Ma and 421 ± 7 Ma (Kirkland et al. 2009) are reflecting the growth of monazite from partial melt. Similar monazite ages of 438 ± 4 Ma and 424 ± 6 Ma are also recorded in sheared migmatite farther south in the Seve Nappe Complex of the Middle Allochthon (Majka et al. 2012).

Concurrent ages of migmatization are insufficient to clearly ascribe the Skibotn Nappe Complex to the Middle Allochthon. The lack of constraints on the pre-migmatitic evolution of the gneisses of the Kåfjord Nappe precludes any comparison with

earlier Caledonian events. Nevertheless, comparable timing of high amphibolite to granulite facies metamorphic event across the Kalak and the Skibotn Nappe Complexes suggest their similar tectonic position at around 445–440 Ma. A lack of a clear suture zone between these two complexes supports their coherent tectonometamorphic evolution from the Late Ordovician to the Early Silurian. Therefore, the similar evolution of the Skibotn and the Kalak Nappe Complexes may support the Baltican affinity of both units. This would be in agreement with the development of the overlying Lyngen Nappe Complex, in the lower part composed of fore-arc lithologies separated by the shear zone from the upper part which is of back-arc origin (Kvassnes et al. 2004). The Lyngen Nappe Complex would therefore represent a fragment of a suture between the Tromsø Nappe Complex of Laurentian origin and the Skibotn Nappe Complex of Baltic affinity. However, there is no evidence of pre-Silurian high pressure metamorphism in the Skibotn Nappe Complex, a feature characteristic for the highest grade units of the Middle Allochthon. Pre-Caledonian metamorphic and magmatic evolution of the Kalak Nappe Complex is also somewhat different from that of other units of the Middle Allochthon (Kirkland et al. 2008; Gasser et al. 2015).

Information about the pre-migmatitic evolution of the Skibotn Nappe Complex is limited to the late Neoproterozoic magmatic age of the Rappesvare granite (Corfu et al. 2007) and the late Cambrian age of a metadiorite in Heia, leaving a certain degree of uncertainty about its exotic origin with respect to the Baltica-derived allochthons (Andresen 1988).

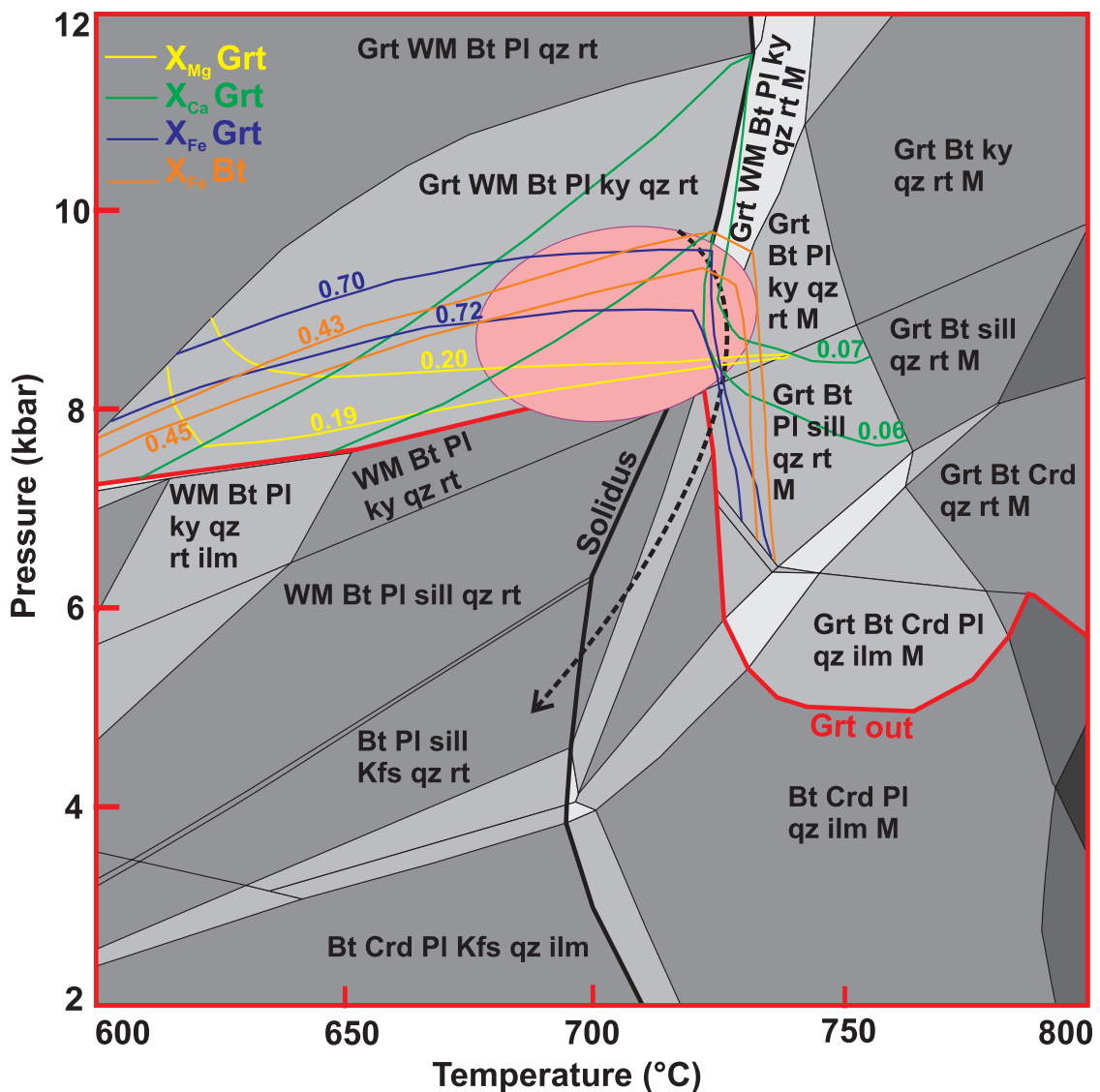


Fig. 10. P-T section for the Kåfjord gneiss (sample JM13-6A) with compositional isopleths of garnet and biotite. Estimated P-T conditions (ellipse) and exhumation P-T path (dashed arrow) of the rock are also shown. For more detail see the text.

Timing of partial melting in the Skibotn Nappe Complex and the Kalak Nappe Complex predates the mafic intrusions emplaced in both complexes (e.g., the Halti Igneous Complex of 434 ± 5 Ma within the Kalak Nappe; Vaajoki & Sipila 2001, the Kågen Gabbro of 435 ± 1 Ma within the Vaddas Nappe; Faber et al. 2019). An extension required for the formation of mafic intrusions of such age is unlikely to occur in the subducted Baltic margin. However, it is a commonly observed phenomenon in the Upper Allochthon in the southern and central parts of the Scandinavian Caledonides (Stephens & Gee 1985; Slagstad & Kirkland 2017). The proposal of a non-Baltic affinity of the Skibotn Nappe Complex and the Kalak Nappe Complex is therefore justified following the general model for the Laurentia–Baltica collision presented by Slagstad and Kirkland (2017). A simplified sketch applying the model to the situation in the Norwegian Arctic Caledonides is presented in Figure 11a. Oceanic crust and partly

continental–oceanic transition zone of the Baltoscandian margin is being subducted underneath Laurentia at ca. 450–440 Ma with subsequent exhumation of the HP rocks and continuous migmatization in the overriding plate including the Skibotn Nappe and Upper Kalak Nappe Complexes. Exhumation of continental crust fragments leads to roll back of the subducting Baltoscandian slab, resulting in extension of the overriding plate manifested by emplacement of mafic intrusions at ca. 440–430 Ma. The Scandian collision between Baltica and Laurentia occurred at ca. 430–415 Ma when the nappe stack emplacement was documented in form of fluid assisted growth of monazite in the Skibotn and the Kalak Nappe Complexes and intrusion of synorogenic granites in the Balsfjord Group.

The model would indicate that the Skibotn Nappe Complex together with the Upper Kalak Nappe Complex was positioned in the overriding plate as the other rocks intruded by

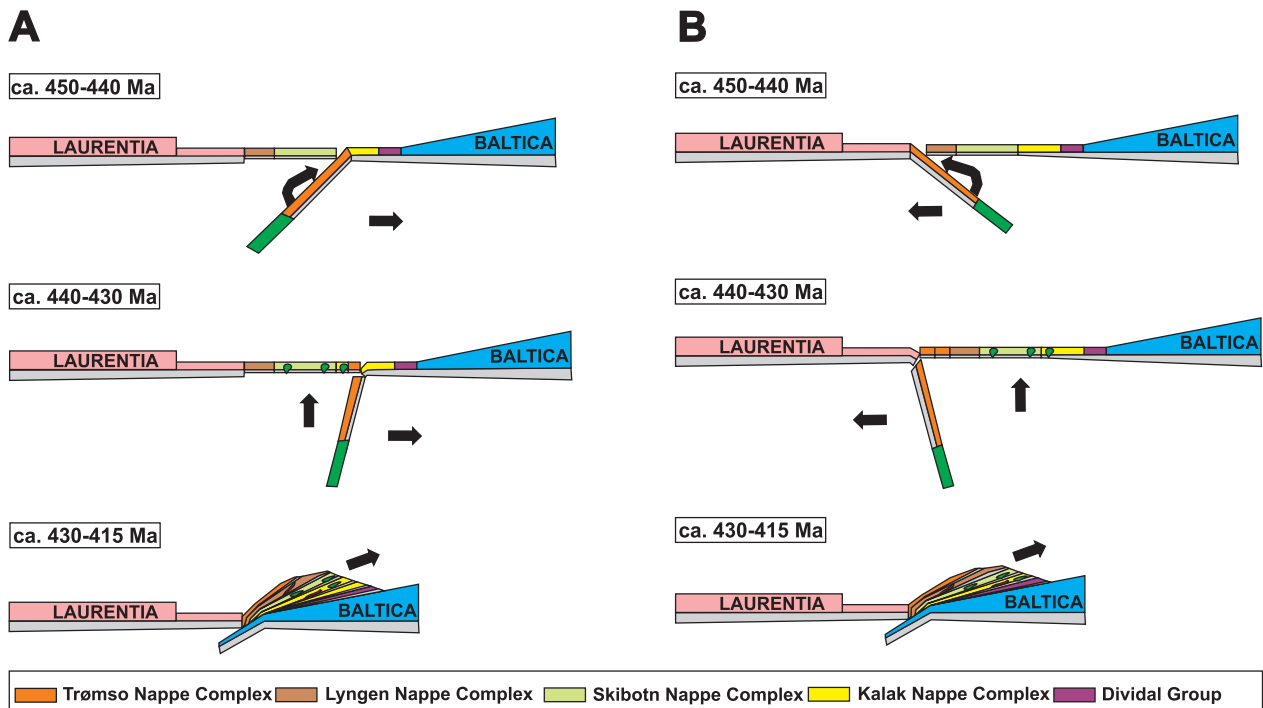


Fig. 11. Schematic sketch of tectonic evolution of the Norwegian Arctic Caledonides at 450–415 Ma: **A** (after Slagstad & Kirkland 2018): I — Baltoscandian margin subducted underneath Laurentia; exhumation of HP lithologies; II — slab roll back and formation of extensional basin in the Laurentian margin; III — Scandian collision resulting in nappe emplacement and synorogenic intrusions; **B** (after Andréasson et al. 2003): I — Laurentian margin subducted underneath Baltica; exhumation of HP lithologies; II — slab roll back and formation of extensional basin in the Baltic margin; III — Scandian collision resulting in nappe emplacement and synorogenic intrusions.

ca. 440–430 Ma mafic intrusions ascribed to the Upper Allochthon to the south. It would also imply that the Trømsø Nappe Complex containing ca. 452 Ma UHP eclogites was a part of the Baltoscandian margin that was thrusted out-of-sequence onto the Baltic plate.

Alternative model including the Skibotn Nappe Complex as a part of an extensional basin formed on Baltoscandian margin was proposed by Andréasson et al. (2003). It provides other possible explanation of the migmatization predating mafic intrusives in the Skibotn-Kalak nappes (Fig. 11b). In this model, Laurentian margin is being subducted underneath Baltic margin and outboard terranes at ca. 450–440 Ma causing migmatization in the overriding plate including the Skibotn Nappe Complex and Upper Kalak Nappe Complexes. Subsequent exhumation of the fragments of subducting plate allows roll back of the Laurentian slab resulting in extension and emplacement of mafic intrusives at ca. 440–430 Ma. As shown in Figure 11a, the Scandian collision between Baltica and Laurentia occurred at ca. 430–415 Ma.

The model presented in Figure 11b is placing both the Skibotn and Kalak Nappe Complexes at ca. 435 Ma in the extensional Baltoscandian margin, however, their affinity to Baltica or Laurentia remains unclear due to inconclusive information about their pre-Silurian evolution. In that scenario, out-of-sequence thrusting is not required for the emplacement of the Tromsø Nappe Complex.

Final remarks

Monazite chemical dating provides new data on the evolution of the migmatitic gneisses of the Kåfjord Nappe. Timing of the prograde phase of migmatitization dated on two samples from the same unit is 444 ± 12 Ma and 442 ± 6.5 Ma. Calculated peak pressure–temperature conditions for this event are 8–10 kbar and 680–720 °C. Late monazite growth at 419 ± 8 Ma and 416 ± 6.9 Ma is interpreted to be associated with the final stages of nappe emplacement.

Obtained monazite ages are comparable with the results from the Kalak Nappe Complex and suggest common evolution of these units from the late Ordovician to the late Silurian. The position of the Kåfjord Nappe as a part of the Middle or Upper Allochthon remains unclear in the light of the geological record of surrounding units.

Acknowledgements: The authors are grateful to Kåre Kullerud for his great help, discussions during the fieldwork, and constructive review of the manuscript. Patrik Konečný is thanked for his assistance during monazite dating. Adam Włodek is acknowledged for his assistance during microprobe analysis. The work was supported by National Science Centre (Poland) “CALSUB” research project no. 2014/14/E/ST10/00321, AGH research grant no. 16.16.140.315, the Slovak Research and Development Agency under the Contract no. APVV-18-0107 and Vega projects 0008/19, 0060/16.

References

- Andresen A. 1988: Caledonian terranes of Northern Norway and their characteristics. *Trabajos de geología* 17, 103–117.
- Andresen A. & Steltenpohl M. G. 1994: Evidence for ophiolite obduction, terrane accretion and polyorogenic evolution of the north Scandinavian Caledonides. *Tectonophysics* 231, 1–3, 59–70. [https://doi.org/10.1016/0040-1951\(94\)90121-X](https://doi.org/10.1016/0040-1951(94)90121-X)
- Andréasson P.G., Svenningsen O.M. & Albrecht L. 1998: Dawn of Phanerozoic orogeny in the North Atlantic tract; evidence from the Seve-Kalak Superterrane, Scandinavian Caledonides. *GFF* 120, 2, 159–172. <https://doi.org/10.1080/11035899801202159>
- Andréasson P.G., Gee D.G., Whitehouse M.J. & Schöberg H. 2003: Subduction-flip during Iapetus Ocean closure and Baltica-Laurentia collision, Scandinavian Caledonides. *Terra Nova* 15, 6, 362–369. <https://doi.org/10.1046/j.1365-3121.2003.00486.x>
- Augland L.E., Andresen A., Gasser D. & Steltenpohl M.G. 2014: Early Ordovician to Silurian evolution of exotic terranes in the Scandinavian Caledonides of the Ofoten–Troms area–terrane characterization and correlation based on new U–Pb zircon ages and Lu–Hf isotopic data. *Geol. Soc. London, Spec. Publ.* 390, 1, 655–678. <https://doi.org/10.1144/SP390.19>
- Bergh S.G. & Andresen A. 1985: Tectonometamorphic evolution of the allochthonous Caledonian rocks between Malangen and Balsfjord, Troms, North Norway. *Universitetsforlaget*, 1–38.
- Binns R.E. 1978: Caledonian nappe correlation and orogenic history in Scandinavia north of lat 67 N. *Geol. Soc. Am. Bull.* 89, 10, 1475–1490.
- Caddick M.J., Konopásek J. & Thompson A.B. 2010: Preservation of garnet growth zoning and the duration of prograde metamorphism. *J. Petrol.* 51, 11, 2327–2347.
- Connolly J.A.D. 1990: Multivariable phase diagrams: an algorithm based on generalized thermodynamics. *Am. J. Sci.* 290, 666–718. <https://doi.org/10.2475/ajs.290.6.666>
- Connolly J.A. 2005: Computation of phase equilibria by linear programming: a tool for geodynamic modeling and its application to subduction zone decarbonation. *Earth Planet. Sci. Lett.* 236, 1–2, 524–541. <https://doi.org/10.1016/j.epsl.2005.04.033>
- Corfu F., Ravna E.J.K. & Kullerud K. 2003: A Late Ordovician U–Pb age for the Tromsø Nappe eclogites, uppermost allochthon of the Scandinavian Caledonides. *Contrib. Mineral. Petrol.* 145, 4, 502–513.
- Corfu F., Roberts R.J., Torsvik T.H., Ashwal L.D. & Ramsay D.M. 2007: Peri-Gondwanan elements in the Caledonian Nappes of Finnmark, Northern Norway: Implications for the paleogeographic framework of the Scandinavian Caledonides. *Am. J. Sci.* 307, 2, 434–458. <https://doi.org/10.2475/02.2007.05>
- Dallmeyer R.D. & Andresen A. 1992: Polyphase tectonothermal evolution of exotic caledonian nappes in Troms, Norway: Evidence from $^{40}\text{Ar}/^{39}\text{Ar}$ mineral ages. *Lithos* 29, 1–2, 19–42. [https://doi.org/10.1016/0024-4937\(92\)90032-T](https://doi.org/10.1016/0024-4937(92)90032-T)
- Dangla P., Démangé J.C., Ploquin A., Quernadel J.M. & Sonet J. 1978: Données géochronologiques sur les Calédonides Scandinaves septentrionales (Troms, Norvège du Nord): *C. r. Acad. Sci. Paris*, 286 D, 1653–1656.
- Dumond G., McLean N., Williams M.L., Jercinovic M.J. & Bowring S.A. 2008: High-resolution dating of granite petrogenesis and deformation in a lower crustal shear zone: Athabasca granulite terrane, western Canadian Shield. *Chem. Geol.* 254, 3–4, 175–196. <https://doi.org/10.1016/j.chemgeo.2008.04.014>
- Elvevold S. 1988: Petrologiske undersøkelser av Kaledonske bergarter i Takvatnområdet, Troms. *Unpublished cand. scient. thesis, University of Tromsø*, 1–149.
- Faber C., Stünitz H., Gasser D., Jeřábek P., Kraus K., Corfu F., Ravna E. & Konopásek J. 2019: Anticlockwise metamorphic pressure–temperature paths and nappe stacking in the Reisa Nappe Complex in the Scandinavian Caledonides, northern Norway: evidence for weakening of lower continental crust before and during continental collision. *Solid Earth* 10, 1, 117–148. <https://doi.org/10.5194/se-10-117-2019>
- Franz G., Andrehs G. & Rhede D. 1996: Crystal chemistry of monazite and xenotime from Saxothuringian–Moldanubian metapelites, NE Bavaria, Germany. *Eur. J. Miner.* 8, 5, 1097–1118.
- Gasser D., Jeřábek P., Faber C., Stünitz H., Menegon L., Corfu F., Erambert M. & Whitehouse M.J. 2015: Behaviour of geochronometers and timing of metamorphic reactions during deformation at lower crustal conditions: phase equilibrium modelling and U–Pb dating of zircon, monazite, rutile and titanite from the Kalak Nappe Complex, northern Norway. *J. Metamorph. Geol.* 33, 5, 513–534. <https://doi.org/10.1111/jmg.12131>
- Gayer R.A., Hayes S.J. & Rice A.H.N. 1985: The structural development of the Kalak Nappe Complex of eastern and central Porsangerhalvøya, Finnmark, Norway. *Norges geologiske Undersøkelse Bulletin* 400, 67–87.
- Gee D.G. 1975: A tectonic model for the central part of the Scandinavian Caledonides. *Am. J. Sci.* 275(A), 468–515.
- Gee D.G., Fossen H., Henriksen N. & Higgins A.K. 2008: From the early Paleozoic platforms of Baltica and Laurentia to the Caledonide Orogen of Scandinavia and Greenland. *Episodes* 31, 1, 44–51.
- Gee D.G., Janák M., Majka J., Robinson P. & van Roermund H. 2013: Subduction along and within the Baltoscandian margin during closing of the Iapetus Ocean and Baltica-Laurentia collision. *Lithosphere* 5, 2, 169–178.
- Harlov D.E., Wirth R. & Förster H.J. 2005: An experimental study of dissolution–reprecipitation in fluorapatite: fluid infiltration and the formation of monazite. *Contrib. Mineral. Petrol.* 150, 268–286.
- Holland T.I.M. & Powell R. 2001: Calculation of phase relations involving haplogranitic melts using an internally consistent thermodynamic dataset. *J. Petrol.* 42, 4, 673–683. <https://doi.org/10.1093/petrology/42.4.673>
- Holland T.J.B. & Powell R. 2011: An improved and extended internally consistent thermodynamic dataset for phases of petrological interest, involving a new equation of state for solids. *J. Metamorph. Geol.* 29, 3, 333–383.
- Indares A. & Dunning G. 2001: Partial melting of high-P–T metapelites from the Tshenukutish Terrane (Grenville Province): petrography and U–Pb geochronology. *J. Petrol.* 42, 8, 1547–1565. <https://doi.org/10.1093/petrology/42.8.1547>
- Janák M., Ravna E.J.K. & Kullerud K. 2012: Constraining peak P–T conditions in UHP eclogites: calculated phase equilibria in kyanite-and phengite-bearing eclogite of the Tromsø Nappe, Norway. *J. Metamorph. Geol.* 30, 4, 377–396. <https://doi.org/10.1111/j.1525-1314.2011.00971.x>
- Janák M., Krogh Ravna E.J., Kullerud K., Yoshida K., Milovský R., & Hirajima T. 2013: Discovery of diamond in the Tromsø Nappe, Scandinavian Caledonides (N. Norway). *J. Metamorph. Geol.* 31, 6, 691–703. <https://doi.org/10.1111/jmg.12040>
- Janots E., Engi M., Berger A., Allaz J., Schwarz J.O. & Spandler C. 2008: Prograde metamorphic sequence of REE minerals in pelitic rocks of the Central Alps: implications for allanite–monazite–xenotime phase relations from 250 to 610 °C. *J. Metamorph. Geol.* 26, 5, 509–526. <https://doi.org/10.1111/j.1525-1314.2008.00774.x>
- Kirkland C.L., Stephen Daly J., & Whitehouse M.J. 2007: Provenance and terrane evolution of the Kalak Nappe Complex, Norwegian Caledonides: implications for Neoproterozoic paleogeography and tectonics. *J. Geol.* 115, 1, 21–41.

- Kirkland C.L., Daly J.S. & Whitehouse M.J. 2008: Basement-cover relationships of the Kalak Nappe Complex, Arctic Norwegian Caledonides and constraints on Neoproterozoic terrane assembly in the North Atlantic region. *Precambrian Res.* 160, 3–4, 245–276. <https://doi.org/10.1016/j.precamres.2007.07.006>
- Kirkland C.L., Whitehouse M.J. & Slagstad T. 2009: Fluid-assisted zircon and monazite growth within a shear zone: a case study from Finnmark, Arctic Norway. *Contrib. Mineral. Petrol.* 158, 5, 637–657.
- Konečný P., Kusiak M.A. & Dunkley D.J. 2018: Improving U–Th–Pb electron microprobe dating using monazite age references. *Chem. Geol.* 484, 22–35.
- Kvassnes A.J., Strand A.H., Moen-Eikeland H. & Pedersen R.B. 2004: The Lyngen gabbro: the lower crust of an Ordovician incipient arc. *Contrib. Mineral. Petrol.* 148, 3, 358–379.
- Lanari P., Vidal O., De Andrade V., Dubacq B., Lewin E., Grosch E. & Schwartz S. 2014: XMapTools: a MATLAB®-based program for electron microprobe X-ray image processing and geothermobarometry. *Comp. Geosci.* 62, 227–240. <https://doi.org/10.1016/j.cageo.2013.08.010>
- Lanari P., Vho A., Bovay T., Airaghi L. & Centrella S. 2019: Quantitative compositional mapping of mineral phases by electron probe micro-analyser. *Geol. Soc. London, Spec. Publ.* 478, SP478-4. <https://doi.org/10.1144/SP478.4>
- Lanzirotti A. & Hanson G.N. 1996: Geochronology and geochemistry of multiple generations of monazite from the Wepawaug Schist, Connecticut, USA: implications for monazite stability in metamorphic rocks. *Contrib. Mineral. Petrol.* 125, 4, 332–340.
- Lindahl I., Stevens B.P. & Zwaan K.B. 2005: The geology of the Vaddas area, Troms: a key to our understanding of the Upper Allochthon in the Caledonides of northern Norway. *Norges Geol. Undersokelse* 445, 5.
- Lindstrøm M. & Andresen A. 1992: Early Caledonian high-grade metamorphism within exotic terranes of the Troms Caledonides. *Norsk Geologisk Tidsskrift* 72, 375–379.
- Majka J., Be’eri-Shlevin Y., Gee D.G., Ladenberger A., Claesson S., Konečný P. & Klonowska I. 2012: Multiple monazite growth in the Åreskutan migmatite: evidence for a polymetamorphic Late Ordovician to Late Silurian evolution in the Seve Nappe Complex of west-central Jamtland, Sweden. *J. Geosci.* 57, 1, 3–23. <http://dx.doi.org/10.3190/jgeosci.112>
- Montel J.M., Foret S., Veschambre M., Nicollet C. & Provost A. 1996: Electron microprobe dating of monazite. *Chem. Geol.* 131, 1–4, 37–53.
- Newton R.C., Charlu T.V. & Kleppa O.J. 1980: Thermochemistry of the high structural state plagioclases. *Geochim. Cosmochim. Acta* 44, 7, 933–941.
- Oliver G.J.H. & Krogh T.E. 1995: U–Pb zircon age of 469 ± 5 Ma for a metatonalite from the Kjosen Unit of the Lyngen Magmatic Complex northern Norway. *Norges Geol. Undersokelse* 428, 27–32.
- Pan Y. 1997: Zircon-and monazite-forming metamorphic reactions at Manitouwadge, Ontario. *Can. Mineral.* 35, 1, 105–118.
- Pedersen R.B., Bruton D.L. & Furnes H. 1992: Ordovician faunas, island arcs and ophiolites in the Scandinavian Caledonides. *Terra Nova* 4, 2, 217–222. <https://doi.org/10.1111/j.1365-3121.1992.tb00475.x>
- Pyle J.M. & Spear F.S. 1999: Yttrium zoning in garnet: coupling of major and accessory phases during metamorphic reactions. *Geol. Mater. Res.* 1, 6, 1–49.
- Pyle J.M., Spear F.S., Rudnick R.L. & McDonough W.F. 2001: Monazite–xenotime–garnet equilibrium in metapelites and a new monazite–garnet thermometer. *J. Petrol.* 42, 11, 2083–2107.
- Ramsay D.M. & Sturt B.A. 1986: The contribution of the Finnmarkian orogeny to the framework of the Scandinavian Caledonides. In: Synthesis of the Caledonian rocks of Britain. Springer, Dordrecht, 221–246.
- Ramsay D.M., Sturt B.A., Roberts D. & Zwaan K.B. 1985: The tectonostratigraphic correlation of the Finnmarkian Nappe Complex. In: Gee D.G. & Sturt B.A. (Eds.): The Caledonide Orogen – Scandinavia and related areas. John Wiley & Sons, Chichester, 163–184.
- Ravna E.K. & Roux M.R.M. 2006: Metamorphic Evolution of the Tønsvika Eclogite, Tromsø Nappe — Evidence for a New UHPM Province in the Scandinavian Caledonides. *Inter. Geol. Rev.* 48, 10, 861–881. <https://doi.org/10.2747/0020-6814.48.10.861>
- Roberts D. & Gee D.G. 1985: An introduction to the structure of the Scandinavian Caledonides. *The Caledonide orogen — Scandinavia and related areas* 1, 55–68.
- Selbekk R.S., Skjerlie K.P. & Pedersen R.B. 2000: Generation of anorthositic magma by H_2O -fluxed anatexis of silica-undersaturated gabbro: an example from the north Norwegian Caledonides. *Geol. Mag.* 137, 6, 609–621.
- Siedlecka A., Roberts D., Nystuen J.P. & Olovyanishnikov V.G. 2004: Northeastern and northwestern margins of Baltica in Neoproterozoic time: evidence from the Timanian and Caledonian Orogens. *Geol. Soc. London, Mem.* 30, 1, 169–190. <https://doi.org/10.1144/GSL.MEM.2004.030.01.15>
- Slagstad T. & Kirkland C.L. 2017: The use of detrital zircon data in terrane analysis: A nonunique answer to provenance and tectonostratigraphic position in the Scandinavian Caledonides. *Lithosphere* 9, 6, 1002–1011. <https://doi.org/10.1130/L663.1>
- Spear F.S. 1988: Metamorphic fractional crystallization and internal metasomatism by diffusional homogenization of zoned garnets. *Contrib. Mineral. Petrol.* 99, 4, 507–517.
- Spear F.S. 2010: Monazite–allanite phase relations in metapelites. *Chem. Geol.* 279, 1–2, 55–62. <https://doi.org/10.1016/j.chemgeo.2010.10.004>
- Stephens M.B. & Gee D.G. 1985: A tectonic model for the evolution of the eugeoclinal terranes in the central Scandinavian Caledonides. In: The Caledonide Orogen: Scandinavia and Related Areas. Wiley, Chichester, 953–978.
- Stephens M.B. & Gee D.G. 1989: Terranes and polyphase accretionary history in the Scandinavian Caledonides. *Geol. Soc. Am., Spec. Pap.* 230, 17–30.
- Sturt B.A. & Roberts D. 1991: Tectonostratigraphic relationships and obduction histories of Scandinavian ophiolitic terranes. In: Ophiolite genesis and evolution of the oceanic lithosphere. Springer, Dordrecht, 745–769.
- Thompson J.B. & Hovis G.L. 1979: Entropy of mixing in sanidine. *Am. Mineral.* 64, 1–2, 57–65.
- Tracy R.J., Robinson P. & Thompson A.B. 1976: Garnet composition and zoning in the determination of temperature and pressure of metamorphism, central Massachusetts. *Am. Mineral.* 61, 7–8, 762–775.
- Vaasjoki M. & Sipila P. 2001: U–Pb isotopic determinations on baddeleyite and zircon from the Halti-Ridnitsohkka intrusion in Finnish Lapland: a further constraint on Caledonide evolution. *Spec. Pap. Geol. Survey Finland* 33, 247–254. <https://doi.org/10.1046/j.0263-4929.2000.00303.x>
- White R.W., Powell R., Holland T.J.B., Johnson T.E. & Green E.C. R. 2014: New mineral activity — composition relations for thermodynamic calculations in metapelite systems. *J. Metamorph. Geol.* 32, 3, 261–286. <https://doi.org/10.1111/jmg.12071>
- Whitney D.L. & Evans B.W. 2010: Abbreviations for names of rock-forming minerals. *Am. Mineral.* 95, 1, 185–187. <https://doi.org/10.2138/am.2010.3371>
- Zwaan K.B. & Roberts D. 1978: Tectonostratigraphic succession and development of the Finnmarkian nappe sequence, North Norway. *Norges Geologiske Undersøkelse* 343, 55–71.

Supplement

Table S1: Chemical analyses of monazite in wt. %. Al and As were analyzed and found below detection (b.d. = below detection, n.a. = not analysed).

Sample name	Analysis No	Note	P ₂ O ₅	PbO	ThO ₂	UO ₂	Y ₂ O ₃	La ₂ O ₃	Ce ₂ O ₃	Pr ₂ O ₃	Nd ₂ O ₃	Sm ₂ O ₃	Eu ₂ O ₃	Gd ₂ O ₃	Tb ₂ O ₃	Dy ₂ O ₃	Ho ₂ O ₃	Er ₂ O ₃	Tm ₂ O ₃	Yb ₂ O ₃	Lu ₂ O ₃	FeO	SO ₃	CaO	SiO ₂	SrO	Total
JM-13-6A	mnz1/1		29.89	0.11	4.28	0.56	3.06	12.48	26.78	3.09	11.32	1.92	0.37	1.37	0.14	0.91	0.12	0.52	0.12	0.14	0.20	0.26	0.20	1.36	0.17	n.a.	99.38
JM-13-6A	mnz1/2		29.75	0.11	4.19	0.66	2.98	12.76	27.00	3.09	11.45	1.88	0.40	1.15	0.09	0.80	b.d.	0.37	0.11	0.17	0.09	0.47	0.18	1.28	0.23	n.a.	99.21
JM-13-6A	mnz4/2		29.55	0.10	3.53	0.49	1.91	13.12	27.83	3.23	12.08	2.03	0.33	1.32	0.09	0.71	b.d.	0.40	0.07	0.11	0.10	0.20	0.04	0.81	0.24	n.a.	98.29
JM-13-6A	mnz7/1		30.48	0.11	4.11	0.50	1.63	12.81	28.48	3.39	13.21	2.24	0.32	1.61	0.15	0.71	b.d.	0.38	0.11	0.08	0.11	b.d.	0.15	1.14	0.27	n.a.	101.99
JM-13-6A	mnz7/2		29.54	0.11	4.46	0.45	1.38	13.09	28.22	3.39	12.72	2.07	0.38	1.42	0.15	0.55	b.d.	0.35	0.17	0.13	b.d.	b.d.	0.17	1.19	0.24	n.a.	100.17
JM-13-6A	mnz7/3		29.96	0.12	4.82	0.66	2.97	12.25	26.60	3.22	12.07	2.22	0.31	1.61	0.16	0.89	b.d.	0.48	0.09	0.17	0.11	b.d.	0.16	1.36	0.23	n.a.	100.45
JM-13-6A	mnz13/1		29.47	0.13	5.02	0.61	1.15	12.85	27.61	3.27	12.67	2.22	0.31	1.38	0.09	0.52	b.d.	0.30	0.06	0.15	0.09	b.d.	0.20	1.43	0.27	n.a.	99.80
JM-13-6A	mnz13/2		29.99	0.11	4.35	0.49	1.61	12.67	27.47	3.26	12.39	2.21	0.34	1.41	0.09	0.59	b.d.	0.39	0.12	0.14	0.09	0.06	0.22	1.29	0.22	n.a.	99.51
JM-13-6A	mnz13/3		30.18	0.12	4.48	0.65	3.00	12.06	26.61	3.21	12.42	2.22	0.38	1.63	0.16	0.86	b.d.	0.44	0.09	0.19	0.11	0.03	0.19	1.33	0.20	n.a.	100.59
JM-13-6A	mnz13/4		29.99	0.11	4.16	0.59	2.72	12.23	26.82	3.21	12.29	2.26	0.33	1.54	0.12	0.90	b.d.	0.44	0.11	0.15	b.d.	0.19	0.15	1.20	0.22	n.a.	99.73
JM-13-6A	mnz14/1		30.07	0.10	3.81	0.56	2.44	12.48	27.30	3.23	12.51	2.24	0.40	1.46	0.13	0.77	b.d.	0.49	0.10	0.16	0.11	0.14	0.20	1.18	0.19	n.a.	100.09
JM-13-6A	mnz14/2		29.59	0.09	3.92	0.42	1.22	12.56	28.26	3.28	12.91	2.38	0.47	1.56	0.13	0.58	b.d.	0.31	0.09	0.12	0.06	0.41	0.09	1.09	0.29	n.a.	99.83
JM-13-6A	mnz15/1		29.32	0.10	3.26	0.54	2.19	13.33	28.74	3.15	11.98	1.87	0.26	1.09	0.09	0.71	b.d.	0.49	0.10	0.13	0.12	b.d.	0.03	0.79	0.22	n.a.	98.49
JM-13-6A	mnz16/1		29.13	0.10	3.63	0.64	2.25	12.87	27.90	3.23	12.14	1.96	0.33	1.12	0.12	0.77	b.d.	0.48	0.08	0.15	0.10	b.d.	0.04	0.88	0.22	n.a.	98.13
JM-13-6A	mnz16/2		29.24	0.11	4.50	0.59	2.06	12.83	27.72	3.18	12.13	1.87	0.35	1.15	0.14	0.72	b.d.	0.45	0.12	0.16	b.d.	b.d.	0.03	1.00	0.28	n.a.	98.64
JM-13-6A	mnz16/3		28.65	0.09	3.47	0.49	2.13	13.00	27.14	3.22	11.83	1.84	0.34	1.14	0.10	0.68	0.09	0.42	0.09	0.12	b.d.	b.d.	0.06	0.90	0.24	n.a.	96.07
JM-13-6A	mnz16/4		28.89	0.11	3.83	0.67	2.29	12.85	27.52	3.26	11.95	1.88	0.33	1.15	0.10	0.75	b.d.	0.41	0.09	0.16	0.09	b.d.	0.03	0.93	0.25	n.a.	97.54
JM-13-6A	mnz18/1		28.81	0.10	4.03	0.46	2.34	12.64	26.95	3.15	11.67	2.01	0.32	1.30	0.12	0.75	0.10	0.40	0.12	0.15	0.09	b.d.	0.06	1.01	0.25	n.a.	96.83
JM-13-6A	mnz18/2		28.51	0.09	3.95	0.43	2.22	12.89	27.22	3.12	11.66	1.91	0.30	1.20	0.10	0.73	b.d.	0.33	0.11	0.14	0.09	b.d.	0.05	0.98	0.27	n.a.	96.30
JM-13-6A	mnz18/3		29.09	0.10	4.14	0.42	2.29	12.71	27.27	3.19	12.04	1.95	0.33	1.27	0.14	0.77	0.12	0.45	0.11	0.14	0.12	b.d.	0.05	0.96	0.24	n.a.	97.89
JM-13-6A	mnz18/4		29.33	0.10	4.01	0.62	2.37	12.53	26.93	3.21	12.24	1.95	0.32	1.18	0.12	0.81	b.d.	0.50	0.13	0.16	0.08	b.d.	0.04	0.95	0.23	n.a.	97.81
SKI-1/13	m1/1		28.48	0.15	4.28	1.14	3.05	12.52	26.66	3.15	12.03	2.16	0.12	1.54	0.22	0.89	0.09	0.50	0.10	0.16	0.06	0.03	n.a.	1.18	0.90	0.01	99.41
SKI-1/13	m1/2		28.41	0.14	3.71	1.23	2.45	12.82	27.25	3.21	12.01	2.23	0.16	1.42	0.15	0.83	0.06	0.47	0.11	0.15	0.07	0.00	n.a.	0.99	0.63	0.02	98.51
SKI-1/13	m2/1		30.45	0.15	3.87	1.20	2.77	12.40	27.23	3.22	12.11	2.24	0.10	1.46	0.20	0.93	0.00	0.60	0.15	0.15	0.00	0.12	n.a.	1.15	0.54	0.01	101.04
SKI-1/13	m3/1		30.26	0.09	2.80	0.42	2.47	13.18	28.69	3.41	12.52	2.22	0.13	1.27	0.17	0.86	0.00	0.55	0.11	0.16	0.09	0.00	n.a.	0.66	0.69	0.01	100.78
SKI-1/13	m3/2		29.74	0.11	3.91	0.64	3.14	12.59	27.31	3.25	11.93	2.07	0.17	1.21	0.20	0.87	0.06	0.57	0.14	0.24	0.04	0.00	n.a.	0.94	0.94	0.00	100.06
SKI-1/13	contam. by Ms	m4/1	21.70	0.10	3.41	0.46	1.99	11.43	25.00	3.08	10.84	1.70	0.19	0.89	0.12	0.58	0.07	0.37	0.11	0.17	0.19	0.37	n.a.	0.72	8.56	0.00	92.05
SKI-1/13		m4/2	29.11	0.14	3.48	1.11	2.53	12.04	26.54	3.27	12.55	2.54	0.12	1.55	0.25	0.94	0.08	0.47	0.12	0.18	0.01	0.00	n.a.	0.93	0.30	0.00	98.24
SKI-1/13		m4/3	30.46	0.05	1.48	0.26	2.45	14.40	28.97	3.36	12.32	2.05	0.21	0.85	0.15	0.72	0.10	0.58	0.16	0.20	0.12	0.01	n.a.	0.56	0.17	0.02	99.63
SKI-1/13		m5/1	29.37	0.19	4.75	1.70	2.33	12.67	26.48	3.23	12.07	2.05	0.13	1.22	0.19	0.78	0.12	0.45	0.13	0.19	0.15	1.09	n.a.	1.18	0.58	0.03	101.07
SKI-1/13	m6/1		30.42	0.13	4.11	0.91	3.22	12.38	26.70	3.17	11.77	2.08	0.08	1.16	0.23	0.95	0.15	0.55	0.14	0.27	0.17	0.06	n.a.	0.97	0.36	0.01	100.01
SKI-1/13	m6/2		30.01	0.13	4.09	0.91	3.19	12.55	26.90	3.31	11.78	2.10	0.13	1.26	0.19	0.90	0.07	0.59	0.13	0.17	0.22	0.07	n.a.	0.96	0.35	0.00	99.99
SKI-1/13	m6/3		30.11	0.13	4.33	0.81	2.83	12.66	27.05	3.24	11.82	2.08	0.18	1.22	0.20	0.89	0.14	0.63	0.13	0.14	0.09	0.04	n.a.	0.96	0.35	0.01	100.03
SKI-1/13	m6/4		29.46	0.13	4.28	0.78	2.72	12.56	26.96	3.22	11.83	2.07	0.13	1.15	0.14	0.91	0.08	0.63	0.12	0.19	0.11	0.09	n.a.	1.00	0.35	0.00	98.92

Table S1 (continued)

Sample name	Analysis No	Note	P ₂ O ₅	PbO	ThO ₂	UO ₂	Y ₂ O ₃	La ₂ O ₃	Ce ₂ O ₃	Pr ₂ O ₃	Nd ₂ O ₃	Sm ₂ O ₃	Eu ₂ O ₃	Gd ₂ O ₃	Tb ₂ O ₃	Dy ₂ O ₃	Ho ₂ O ₃	Er ₂ O ₃	Tm ₂ O ₃	Yb ₂ O ₃	Lu ₂ O ₃	FeO	SO ₃	CaO	SiO ₂	SrO	Total
SKI-1/13	m7/1		30.66	0.14	3.77	1.00	2.64	12.86	27.45	3.25	12.06	2.26	0.16	1.33	0.22	0.99	0.11	0.51	0.11	0.12	0.12	0.96	n.a.	0.90	0.33	0.01	101.95
SKI-1/13	m7/2		30.34	0.13	4.03	1.00	2.66	12.55	27.13	3.27	12.10	2.26	0.20	1.37	0.23	0.93	0.07	0.57	0.12	0.16	0.20	0.81	n.a.	0.96	0.39	0.02	101.50
SKI-1/13	m8/1		31.22	0.12	3.60	0.78	2.64	13.99	27.92	3.20	11.44	1.81	0.14	0.87	0.09	0.69	0.10	0.60	0.18	0.20	0.17	0.04	n.a.	0.82	0.33	0.02	100.98
SKI-1/13	m8/2		30.49	0.19	5.41	1.32	3.27	12.92	25.89	3.07	10.90	1.83	0.10	0.95	0.15	0.83	0.09	0.73	0.15	0.24	0.16	0.01	n.a.	1.28	0.40	0.02	100.42
SKI-1/13	m8/3		29.54	0.18	5.23	1.35	3.05	13.23	25.91	2.97	10.62	1.74	0.11	0.84	0.18	0.81	0.12	0.67	0.15	0.18	0.13	0.00	n.a.	1.28	0.42	0.00	98.72
SKI-1/13	m9/1		30.85	0.15	3.85	1.27	2.65	12.47	26.92	3.21	11.79	2.20	0.07	1.27	0.19	0.99	0.05	0.55	0.08	0.14	0.03	0.00	n.a.	1.12	0.37	0.01	100.22
SKI-1/13	m9/2		30.31	0.10	2.79	0.67	4.24	12.57	26.19	3.13	11.45	2.15	0.13	1.22	0.18	1.14	0.18	0.86	0.12	0.32	0.07	0.00	n.a.	1.06	0.01	0.28	99.19
SKI-1/13	m10/1		30.82	0.09	2.68	0.52	2.55	13.40	28.27	3.33	12.29	2.16	0.09	1.14	0.19	0.85	0.00	0.45	0.07	0.19	0.08	0.00	n.a.	0.69	0.24	0.03	100.10
SKI-1/13	m11/1		31.90	0.10	2.33	0.95	3.01	13.48	28.07	3.31	11.98	2.00	0.15	1.04	0.14	0.67	0.12	0.56	0.12	0.24	0.15	0.01	n.a.	0.66	0.01	0.27	101.40
SKI-1/13	m11/2		29.62	0.14	3.52	1.13	3.14	12.72	26.92	3.16	11.80	2.06	0.09	1.23	0.22	0.84	0.03	0.60	0.13	0.18	0.13	0.02	n.a.	0.94	0.34	0.00	98.96
SKI-1/13	m12/1		30.10	0.15	4.77	1.05	3.33	12.28	26.57	3.25	11.91	2.07	0.18	1.32	0.18	0.92	0.05	0.60	0.11	0.23	0.12	0.00	n.a.	1.12	0.49	0.02	100.82
SKI-1/13	m12/2		29.98	0.10	2.81	0.64	2.63	13.43	28.12	3.29	11.89	1.97	0.10	1.17	0.21	0.75	0.14	0.56	0.14	0.12	0.09	0.01	n.a.	0.74	0.35	0.01	99.26
SKI-1/13	m12/3		29.69	0.12	4.01	0.81	2.86	12.74	27.26	3.23	11.82	2.07	0.12	1.13	0.16	0.90	0.03	0.51	0.18	0.15	0.00	0.00	n.a.	0.94	0.45	0.01	99.20
SKI-1/13	m13/1		30.14	0.13	4.00	0.98	2.74	14.31	26.88	3.05	11.01	1.70	0.17	0.84	0.12	0.77	0.01	0.56	0.09	0.18	0.09	0.02	n.a.	0.99	0.34	0.00	99.12
SKI-1/13	m13/2		30.97	0.15	3.86	1.22	3.68	13.78	26.16	2.99	10.89	1.77	0.08	0.94	0.19	0.93	0.05	0.71	0.17	0.18	0.13	0.00	n.a.	1.10	0.27	0.00	100.25
SKI-1/13 A	m1/1		30.16	0.14	3.88	1.07	2.56	12.67	27.19	3.14	11.87	2.14	0.22	1.20	0.16	0.86	0.13	0.50	0.11	0.15	0.16	0.00	n.a.	0.97	0.30	0.00	99.57
SKI-1/13 A	m1/2		30.27	0.15	4.01	1.13	2.57	12.53	26.81	3.11	11.83	2.21	0.14	1.22	0.18	0.85	0.05	0.47	0.12	0.18	0.05	0.00	n.a.	1.12	0.29	0.01	99.31
SKI-1/13 A	m1/3		30.19	0.16	5.10	1.09	3.37	12.09	25.74	3.14	11.40	2.04	0.20	1.17	0.22	1.01	0.02	0.64	0.14	0.21	0.03	0.00	n.a.	1.17	0.37	0.01	99.51
SKI-1/13 A	m1/4		30.17	0.11	3.52	0.76	2.60	12.67	27.42	3.18	12.05	2.14	0.14	1.19	0.18	0.90	0.00	0.52	0.05	0.18	0.10	0.00	n.a.	0.91	0.28	0.00	99.07
SKI-1/13 A	m2/1		30.56	0.09	2.83	0.62	2.68	12.51	27.94	3.32	12.37	2.16	0.18	1.22	0.17	0.71	0.13	0.59	0.08	0.18	0.06	0.00	n.a.	0.66	0.27	0.01	99.34
SKI-1/13 A	m2/2		30.20	0.13	4.12	0.80	2.49	12.51	26.62	3.07	11.59	2.04	0.14	1.17	0.22	0.82	0.17	0.59	0.07	0.16	0.12	0.00	n.a.	0.92	0.39	0.03	98.40
SKI-1/13 A	m3/1		30.48	0.05	2.02	0.22	2.25	14.12	28.82	3.35	12.19	1.95	0.21	0.91	0.11	0.65	0.13	0.48	0.18	0.19	0.14	0.00	n.a.	0.46	0.22	0.00	99.14
SKI-1/13 A	m3/2		30.52	0.09	2.72	0.57	2.37	13.39	27.85	3.23	12.17	2.11	0.15	1.06	0.20	0.82	0.00	0.50	0.09	0.22	0.23	0.00	n.a.	0.75	0.22	0.02	99.28
SKI-1/13 A	m3/3		30.67	0.11	3.50	0.56	3.71	12.80	26.48	3.10	11.65	2.13	0.19	1.29	0.22	1.00	0.11	0.64	0.16	0.23	0.08	0.00	n.a.	1.05	0.23	0.02	99.94
SKI-1/13 A	m4/1		30.57	0.11	4.15	0.74	3.23	13.14	27.11	3.29	11.91	2.10	0.12	1.10	0.18	0.84	0.15	0.57	0.12	0.24	0.06	0.12	n.a.	1.08	0.26	0.01	101.21
SKI-1/13 A	m4/2		30.35	0.19	6.29	1.10	3.57	11.88	24.63	3.03	10.98	2.12	0.13	1.33	0.18	1.08	0.15	0.76	0.15	0.20	0.14	0.08	n.a.	1.37	0.44	0.00	100.19
SKI-1/13 A	m5/1		30.51	0.08	2.93	0.49	2.65	12.98	27.52	3.27	12.18	2.17	0.21	1.11	0.18	0.89	0.05	0.52	0.12	0.17	0.06	0.09	n.a.	0.69	0.27	0.00	99.14
SKI-1/13 A	m5/2		30.37	0.12	4.14	0.55	2.69	12.80	26.42	3.24	11.92	2.10	0.20	1.31	0.14	0.88	0.15	0.49	0.15	0.18	0.09	0.11	n.a.	0.92	0.36	0.02	99.33

Table S2: Chemical analyses of monazite with structural formulae recalculated on the basis of 16 oxygens.

Sample name	Analysis No	P	Pb	Th	U	Y	La	Ce	Pr	Nd	Sm	Eu	Gd	Tb	Dy	Ho	Er	Tm	Yb	Lu	Fe	S	Ca	Si	Sr	Total	X _{mon}	X _{hut}	X _{che}	X _{xno}	Eu/Eu*	Y _N	
JM-13-6A	mnz1/1	3.94	0.00	0.15	0.02	0.25	0.72	1.53	0.18	0.63	0.10	0.02	0.07	0.01	0.05	0.00	0.03	0.01	0.01	0.03	0.02	0.23	0.03	n.a.	8.03	0.84	0.01	0.09	0.06	0.67	19492		
JM-13-6A	mnz1/2	3.93	0.00	0.15	0.02	0.25	0.73	1.54	0.18	0.64	0.10	0.02	0.06	0.01	0.04	0.00	0.02	0.01	0.01	0.00	0.06	0.02	0.21	0.04	n.a.	8.04	0.84	0.01	0.09	0.06	0.77	19001	
JM-13-6A	mnz4/2	3.97	0.00	0.13	0.02	0.16	0.77	1.62	0.19	0.68	0.11	0.02	0.07	0.01	0.04	0.00	0.02	0.00	0.01	0.00	0.00	0.03	0.00	0.14	0.04	n.a.	8.01	0.88	0.01	0.07	0.04	0.57	12161
JM-13-6A	mnz7/1	3.95	0.00	0.14	0.02	0.13	0.72	1.59	0.19	0.72	0.12	0.02	0.08	0.01	0.03	0.00	0.02	0.01	0.00	0.00	0.00	0.02	0.19	0.04	n.a.	8.01	0.87	0.01	0.08	0.03	0.49	10386	
JM-13-6A	mnz7/2	3.92	0.00	0.16	0.02	0.12	0.76	1.62	0.19	0.71	0.11	0.02	0.07	0.01	0.03	0.00	0.02	0.01	0.01	0.00	0.00	0.02	0.20	0.04	n.a.	8.03	0.87	0.01	0.09	0.03	0.64	8792	
JM-13-6A	mnz7/3	3.93	0.01	0.17	0.02	0.24	0.70	1.51	0.18	0.67	0.12	0.02	0.08	0.01	0.04	0.00	0.02	0.00	0.01	0.01	0.00	0.02	0.23	0.04	n.a.	8.03	0.83	0.01	0.10	0.06	0.48	18889	
JM-13-6A	mnz13/1	3.92	0.01	0.18	0.02	0.10	0.74	1.59	0.19	0.71	0.12	0.02	0.07	0.01	0.03	0.00	0.01	0.00	0.01	0.00	0.00	0.02	0.24	0.04	n.a.	8.03	0.86	0.01	0.11	0.02	0.49	7321	
JM-13-6A	mnz13/2	3.96	0.00	0.15	0.02	0.13	0.73	1.57	0.19	0.69	0.12	0.02	0.07	0.01	0.03	0.00	0.02	0.01	0.01	0.00	0.01	0.03	0.22	0.03	n.a.	8.01	0.87	0.01	0.09	0.03	0.54	10242	
JM-13-6A	mnz13/3	3.94	0.00	0.16	0.02	0.25	0.69	1.50	0.18	0.68	0.12	0.02	0.08	0.01	0.04	0.00	0.02	0.00	0.01	0.01	0.00	0.02	0.22	0.03	n.a.	8.02	0.84	0.01	0.09	0.06	0.58	19136	
JM-13-6A	mnz13/4	3.95	0.00	0.15	0.02	0.22	0.70	1.53	0.18	0.68	0.12	0.02	0.08	0.01	0.04	0.00	0.02	0.01	0.01	0.00	0.02	0.20	0.03	n.a.	8.02	0.85	0.01	0.09	0.06	0.52	17301		
JM-13-6A	mnz14/1	3.95	0.00	0.13	0.02	0.20	0.71	1.55	0.18	0.69	0.12	0.02	0.07	0.01	0.04	0.00	0.02	0.00	0.01	0.01	0.02	0.20	0.03	n.a.	8.02	0.86	0.01	0.08	0.05	0.64	15554		
JM-13-6A	mnz14/2	3.93	0.00	0.14	0.01	0.10	0.73	1.62	0.19	0.72	0.13	0.03	0.08	0.01	0.03	0.00	0.02	0.00	0.01	0.00	0.05	0.01	0.18	0.05	n.a.	8.05	0.88	0.01	0.08	0.03	0.70	7751	
JM-13-6A	mnz15/1	3.94	0.00	0.12	0.02	0.19	0.78	1.67	0.18	0.68	0.10	0.01	0.06	0.01	0.04	0.00	0.02	0.00	0.01	0.01	0.00	0.03	0.13	0.03	n.a.	8.01	0.88	0.01	0.06	0.05	0.52	13958	
JM-13-6A	mnz16/1	3.94	0.00	0.13	0.02	0.19	0.76	1.63	0.19	0.69	0.11	0.02	0.06	0.01	0.04	0.00	0.02	0.00	0.01	0.00	0.00	0.15	0.04	n.a.	8.02	0.87	0.01	0.07	0.05	0.62	14312		
JM-13-6A	mnz16/2	3.93	0.00	0.16	0.02	0.17	0.75	1.61	0.18	0.69	0.10	0.02	0.06	0.01	0.04	0.00	0.02	0.01	0.01	0.00	0.00	0.17	0.05	n.a.	8.02	0.86	0.01	0.08	0.04	0.67	13124		
JM-13-6A	mnz16/3	3.94	0.00	0.13	0.02	0.18	0.78	1.62	0.19	0.69	0.10	0.02	0.06	0.01	0.04	0.00	0.02	0.00	0.01	0.00	0.00	0.16	0.04	n.a.	8.02	0.87	0.01	0.07	0.05	0.67	13560		
JM-13-6A	mnz16/4	3.93	0.00	0.14	0.02	0.20	0.76	1.62	0.19	0.69	0.10	0.02	0.06	0.01	0.04	0.00	0.02	0.00	0.01	0.00	0.00	0.16	0.04	n.a.	8.03	0.87	0.01	0.08	0.05	0.63	14615		
JM-13-6A	mnz18/1	3.94	0.00	0.15	0.02	0.20	0.75	1.59	0.19	0.67	0.11	0.02	0.07	0.01	0.04	0.00	0.02	0.01	0.01	0.00	0.01	0.17	0.04	n.a.	8.02	0.86	0.01	0.08	0.05	0.57	14918		
JM-13-6A	mnz18/2	3.93	0.00	0.15	0.02	0.19	0.77	1.62	0.19	0.68	0.11	0.02	0.06	0.01	0.04	0.00	0.02	0.01	0.01	0.00	0.01	0.17	0.04	n.a.	8.03	0.86	0.01	0.08	0.05	0.57	14121		
JM-13-6A	mnz18/3	3.94	0.00	0.15	0.02	0.19	0.75	1.60	0.19	0.69	0.11	0.02	0.07	0.01	0.04	0.00	0.02	0.01	0.01	0.00	0.01	0.16	0.04	n.a.	8.02	0.86	0.01	0.08	0.05	0.61	14557		
JM-13-6A	mnz18/4	3.96	0.00	0.15	0.02	0.20	0.74	1.57	0.19	0.70	0.11	0.02	0.06	0.01	0.04	0.00	0.02	0.01	0.01	0.00	0.00	0.16	0.04	n.a.	8.00	0.86	0.01	0.08	0.05	0.60	15080		
SKI-1/13	m1/1	3.82	0.01	0.15	0.04	0.26	0.73	1.55	0.18	0.68	0.12	0.01	0.08	0.01	0.05	0.00	0.02	0.00	0.01	0.00	0.00	n.a.	0.20	0.14	0.00	8.08	0.84	0.00	0.10	0.06	0.19	15310	
SKI-1/13	m1/2	3.86	0.01	0.14	0.04	0.21	0.76	1.60	0.19	0.69	0.12	0.01	0.08	0.01	0.04	0.00	0.02	0.01	0.01	0.00	0.00	n.a.	0.17	0.10	0.00	8.06	0.86	0.00	0.08	0.05	0.25	12292	
SKI-1/13	m2/1	3.95	0.01	0.14	0.04	0.23	0.70	1.53	0.18	0.66	0.12	0.01	0.07	0.01	0.05	0.00	0.03	0.01	0.01	0.00	0.02	n.a.	0.19	0.08	0.00	8.02	0.85	0.00	0.10	0.06	0.16	13911	
SKI-1/13	m3/1	3.94	0.00	0.10	0.01	0.20	0.75	1.62	0.19	0.69	0.12	0.01	0.06	0.01	0.04	0.00	0.03	0.01	0.01	0.00	0.00	n.a.	0.11	0.11	0.00	8.00	0.89	0.00	0.06	0.05	0.22	12400	
SKI-1/13	m3/2	3.90	0.00	0.14	0.02	0.26	0.72	1.55	0.18	0.66	0.11	0.01	0.06	0.01	0.04	0.00	0.03	0.01	0.01	0.00	0.00	n.a.	0.16	0.15	0.00	8.02	0.85	0.00	0.08	0.07	0.30	15741	
SKI-1/13	m4/1	contaminated																															
SKI-1/13	m4/2	3.94	0.01	0.13	0.04	0.22	0.71	1.55	0.19	0.72	0.14	0.01	0.08	0.01	0.05	0.00	0.02	0.01	0.01	0.00	0.00	n.a.	0.16	0.05	0.00	8.03	0.87	0.00	0.08	0.05	0.17	12703	
SKI-1/13	m4/3	4.00	0.00	0.05	0.01	0.20	0.82	1.65	0.19	0.68	0.11	0.01	0.04	0.01	0.04	0.00	0.03	0.01	0.01	0.01	0.00	n.a.	0.09	0.03	0.00	8.00	0.91	0.00	0.05	0.05	0.40	12295	
SKI-1/13	m5/1	3.87	0.01	0.17	0.06	0.19	0.73	1.51	0.18	0.67	0.11	0.01	0.06	0.01	0.04	0.01	0.02	0.01	0.01	0.01	0.14	n.a.	0.20	0.09	0.00	8.10	0.84	0.01	0.10	0.05	0.24	11705	
SKI-1/13	m6/1	3.98	0.01	0.14	0.03	0.27	0.71	1.51	0.18	0.65	0.11	0.00	0.06	0.01	0.05	0.01	0.03	0.01	0.01	0.01	0.01	n.a.	0.16	0.05	0.00	7.99	0.85	0.01	0.08	0.07	0.14	16169	
SKI-1/13	m6/2	3.95	0.01	0.14	0.03	0.26	0.72	1.53	0.19	0.65	0.11	0.01	0.06	0.01	0.05	0.00	0.03	0.01	0.01	0.01	0.01	n.a.	0.16	0.05	0.00	8.01	0.85	0.01	0.08	0.07	0.22	16004	
SKI-1/13	m6/3	3.96	0.01	0.15	0.03	0.23	0.73	1.54	0.18	0.66	0.11	0.01	0.06	0.01	0.04	0.01	0.03	0.01	0.01	0.00	0.00	n.a.	0.16	0.05	0.00	8.00	0.85	0.01	0.08	0.06	0.31	14195	
SKI-1/13	m6/4	3.94	0.01	0.15	0.03	0.23	0.73	1.56	0.19	0.67	0.11	0.01	0.06	0.01	0.05	0.00	0.03	0.01	0.01	0.01	0.01	n.a.	0.17	0.06	0.00	8.02	0.85	0.00	0.08	0.06	0.24	13652	
SKI-1/13	m7/1	3.96	0.01	0.13	0.03	0.21	0.72	1.53	0.18	0.66	0.12	0.01	0.07	0.01	0.05	0.01	0.02	0.01	0.01	0.													

Table S2 (continued)

Sample name	Analysis No	P	Pb	Th	U	Y	La	Ce	Pr	Nd	Sm	Eu	Gd	Tb	Dy	Ho	Er	Tm	Yb	Lu	Fe	S	Ca	Si	Sr	Total	X _{mon}	X _{hutt}	X _{che}	X _{xno}	Eu/Eu*	Y _N
SKI-1/13	m8/2	3.97	0.01	0.19	0.05	0.27	0.73	1.46	0.17	0.60	0.10	0.01	0.05	0.01	0.04	0.00	0.04	0.01	0.01	0.01	0.00	n.a.	0.21	0.06	0.00	7.99	0.82	0.01	0.11	0.07	0.22	16379
SKI-1/13	m8/3	3.94	0.01	0.19	0.05	0.26	0.77	1.50	0.17	0.60	0.09	0.01	0.04	0.01	0.04	0.01	0.03	0.01	0.01	0.01	0.00	n.a.	0.22	0.07	0.00	8.01	0.82	0.01	0.11	0.06	0.25	15321
SKI-1/13	m9/1	4.01	0.01	0.13	0.04	0.22	0.71	1.51	0.18	0.65	0.12	0.00	0.06	0.01	0.05	0.00	0.03	0.00	0.01	0.00	0.00	n.a.	0.18	0.06	0.00	7.98	0.85	0.00	0.09	0.06	0.12	13282
SKI-1/13	m9/2	3.98	0.00	0.10	0.02	0.35	0.72	1.49	0.18	0.63	0.11	0.01	0.06	0.01	0.06	0.01	0.04	0.01	0.02	0.00	0.00	n.a.	0.18	0.04	0.00	8.02	0.81	0.01	0.09	0.09	0.23	21256
SKI-1/13	m10/1	4.02	0.00	0.09	0.02	0.21	0.76	1.59	0.19	0.68	0.11	0.00	0.06	0.01	0.04	0.00	0.02	0.00	0.01	0.00	0.00	n.a.	0.11	0.04	0.00	7.98	0.89	0.00	0.06	0.05	0.15	12771
SKI-1/13	m11/1	3.94	0.01	0.13	0.04	0.26	0.74	1.55	0.18	0.66	0.11	0.00	0.06	0.01	0.04	0.00	0.03	0.01	0.01	0.01	0.00	n.a.	0.16	0.05	0.00	8.02	0.84	0.01	0.08	0.07	0.15	15121
SKI-1/13	m11/2	3.95	0.01	0.13	0.04	0.26	0.74	1.55	0.18	0.66	0.11	0.00	0.06	0.01	0.04	0.00	0.03	0.01	0.01	0.01	0.00	n.a.	0.16	0.05	0.00	8.02	0.85	0.00	0.08	0.07	0.15	15735
SKI-1/13	m12/1	3.93	0.01	0.17	0.04	0.27	0.70	1.50	0.18	0.66	0.11	0.01	0.07	0.01	0.05	0.00	0.03	0.01	0.01	0.01	0.00	n.a.	0.19	0.08	0.00	8.02	0.83	0.01	0.09	0.07	0.30	16686
SKI-1/13	m12/2	3.97	0.00	0.10	0.02	0.22	0.77	1.61	0.19	0.66	0.11	0.01	0.06	0.01	0.04	0.01	0.03	0.01	0.01	0.01	0.00	n.a.	0.12	0.05	0.00	8.00	0.88	0.00	0.06	0.06	0.19	13201
SKI-1/13	m12/3	3.94	0.01	0.14	0.03	0.24	0.74	1.57	0.18	0.66	0.11	0.01	0.06	0.01	0.05	0.00	0.03	0.01	0.01	0.00	0.00	n.a.	0.16	0.07	0.00	8.01	0.86	0.00	0.08	0.06	0.22	14362
SKI-1/13	m13/1	3.98	0.01	0.14	0.03	0.23	0.82	1.54	0.17	0.61	0.09	0.01	0.04	0.01	0.04	0.00	0.03	0.00	0.01	0.00	0.00	n.a.	0.17	0.05	0.00	7.99	0.85	0.00	0.08	0.06	0.38	13757
SKI-1/13	m13/2	4.01	0.01	0.13	0.04	0.30	0.78	1.47	0.17	0.60	0.09	0.00	0.05	0.01	0.05	0.00	0.03	0.01	0.01	0.01	0.00	n.a.	0.18	0.04	0.00	7.98	0.83	0.00	0.09	0.08	0.18	18468
SKI-1/13A	m1/1	3.98	0.01	0.14	0.04	0.21	0.73	1.55	0.18	0.66	0.11	0.01	0.06	0.01	0.04	0.01	0.02	0.01	0.01	0.01	0.00	n.a.	0.16	0.05	0.00	7.99	0.86	0.00	0.08	0.05	0.38	12843
SKI-1/13A	m1/2	3.99	0.01	0.14	0.04	0.21	0.72	1.53	0.18	0.66	0.12	0.01	0.06	0.01	0.04	0.00	0.02	0.01	0.01	0.00	0.00	n.a.	0.19	0.05	0.00	7.99	0.85	0.00	0.09	0.05	0.24	12904
SKI-1/13A	m1/3	3.97	0.01	0.18	0.04	0.28	0.69	1.47	0.18	0.63	0.11	0.01	0.06	0.01	0.05	0.00	0.03	0.01	0.01	0.00	0.00	n.a.	0.19	0.06	0.00	7.99	0.82	0.01	0.10	0.07	0.36	16879
SKI-1/13A	m1/4	3.99	0.00	0.13	0.03	0.22	0.73	1.57	0.18	0.67	0.11	0.01	0.06	0.01	0.05	0.00	0.03	0.00	0.01	0.01	0.00	n.a.	0.15	0.04	0.00	7.99	0.87	0.00	0.08	0.05	0.24	13054
SKI-1/13A	m2/1	4.01	0.00	0.10	0.02	0.22	0.72	1.59	0.19	0.69	0.12	0.01	0.06	0.01	0.04	0.01	0.03	0.00	0.01	0.00	0.00	n.a.	0.11	0.04	0.00	7.97	0.88	0.00	0.06	0.06	0.30	13445
SKI-1/13A	m2/2	4.01	0.01	0.15	0.03	0.21	0.72	1.53	0.18	0.65	0.11	0.01	0.06	0.01	0.04	0.01	0.03	0.00	0.01	0.01	0.00	n.a.	0.15	0.06	0.00	7.97	0.86	0.01	0.08	0.05	0.26	12502
SKI-1/13A	m3/1	4.02	0.00	0.07	0.01	0.19	0.81	1.64	0.19	0.68	0.10	0.01	0.05	0.01	0.03	0.01	0.02	0.01	0.01	0.01	0.00	n.a.	0.08	0.03	0.00	7.98	0.91	0.00	0.04	0.05	0.41	11276
SKI-1/13A	m3/2	4.02	0.00	0.10	0.02	0.20	0.77	1.59	0.18	0.68	0.11	0.01	0.05	0.01	0.04	0.00	0.02	0.00	0.01	0.01	0.00	n.a.	0.12	0.03	0.00	7.98	0.89	0.00	0.06	0.05	0.26	11902
SKI-1/13A	m3/3	4.00	0.00	0.12	0.02	0.30	0.73	1.49	0.17	0.64	0.11	0.01	0.07	0.01	0.05	0.01	0.03	0.01	0.01	0.00	0.00	n.a.	0.17	0.04	0.00	8.00	0.84	-0.01	0.09	0.08	0.32	18631
SKI-1/13A	m4/1	3.97	0.00	0.14	0.03	0.26	0.74	1.52	0.18	0.65	0.11	0.01	0.06	0.01	0.04	0.01	0.03	0.01	0.01	0.00	0.01	n.a.	0.18	0.04	0.00	8.02	0.85	0.00	0.09	0.07	0.22	16185
SKI-1/13A	m4/2	3.97	0.01	0.22	0.04	0.29	0.68	1.39	0.17	0.61	0.11	0.01	0.07	0.01	0.05	0.01	0.04	0.01	0.01	0.01	0.01	n.a.	0.23	0.07	0.00	8.00	0.80	0.01	0.11	0.07	0.23	17926
SKI-1/13A	m5/1	4.01	0.00	0.10	0.02	0.22	0.74	1.57	0.18	0.68	0.12	0.01	0.06	0.01	0.04	0.00	0.03	0.01	0.01	0.00	0.01	n.a.	0.12	0.04	0.00	7.98	0.88	0.00	0.06	0.06	0.37	13285
SKI-1/13A	m5/2	4.00	0.01	0.15	0.02	0.22	0.73	1.50	0.18	0.66	0.11	0.01	0.07	0.01	0.04	0.01	0.02	0.01	0.01	0.00	0.01	n.a.	0.15	0.06	0.00	7.99	0.86	0.00	0.08	0.06	0.34	13481